INTERNATIONAL TELECOMMUNICATION UNION

CCIR

INTERNATIONAL
RADIO CONSULTATIVE
COMMITTEE

SUPPLEMENT TO REPORT 252-2

SECOND CCIR COMPUTER-BASED INTERIM METHOD FOR ESTIMATING SKY-WAVE FIELD STRENGTH AND TRANSMISSION LOSS AT FREQUENCIES BETWEEN 2 AND 30 MHz

XIVth PLENARY ASSEMBLY
KYOTO, 1978

Geneva, 1980

INTERNATIONAL TELECOMMUNICATION UNION

CCIR

INTERNATIONAL
RADIO CONSULTATIVE
COMMITTEE

SUPPLEMENT TO REPORT 252-2

SECOND CCIR COMPUTER-BASED INTERIM METHOD FOR ESTIMATING SKY-WAVE FIELD STRENGTH AND TRANSMISSION LOSS AT FREQUENCIES BETWEEN 2 AND 30 MHz

(Study Programme 30A/6)

XIVth PLENARY ASSEMBLY
KYOTO, 1978

Geneva, 1980

NOTE BY THE SECRETARIAT

This supplement provides a replacement for Report 252-2; however, Report 252-2 is maintained until this supplement is completed with a suitable computer program.

TABLE OF CONTENTS

Page No.

Symbols used in the text IV

1. Introduction 1

2. Requirements for predictions 1

3. Principles of the method 2

4. Ionospheric characteristics 3
   - 4.1 Monthly median values 3
   - 4.2 Day-to-day scatter statistics and mode availability 5

5. Models of vertical distributions of electron concentration 9

6. Sky-wave paths in the ionosphere 10
   - 6.1 Possible propagation modes 10
   - 6.2 Determination of the MUF 11
   - 6.3 Reflection from the E and F-layers 11
   - 6.4 Reflection from and transmission through the sporadic-E layer 13
   - 6.5 Frequencies above the MUF 13

7. Transmission loss and gain factors 13
   - 7.1 Transmitting and receiving-antenna gains; G_t, G_r 14
   - 7.2 Spatial attenuation, L_{cl} 14
   - 7.3 Ionospheric absorption 15
     - 7.3.1 Non-deviative and deviative absorption, L_a 16
     - 7.3.2 Auroral absorption, L_h 17
   - 7.4 Polarization-coupling loss and multiple-hop ground-reflection loss, L_c 19
     - 7.4.1 Single-hop modes 19
     - 7.4.2 Multiple-hop modes 20
   - 7.5 Sporadic-E obscuration and reflection losses 21
     - 7.5.1 Obscuration loss, L_q 21
     - 7.5.2 Reflection loss, L_r 22
   - 7.6 Loss associated with propagation at frequencies above the MUF, L_m 22
   - 7.7 Additional losses, L_z 23

8. Overall transmission loss and field strength of downcoming sky waves at receiving site 23
   - 8.1 Basic free-space transmission loss, L_{bf} 23
   - 8.2 Basic transmission loss, L_b 23
   - 8.3 Transmission loss, L 23
   - 8.4 System loss, L_s 24
   - 8.5 r.m.s. sky-wave field strength 24
   - 8.6 Fading allowance for conversion from r.m.s. to mean or median sky-wave field strength 24
   - 8.7 Summation of powers in active modes and multipath probability 24
   - 8.8 Day-to-day variations in transmission loss and field strength 25

References 28

Symbols used in the text

Principal loss and gain factors

(All factors are expressed in decibels; f is the wave frequency in MHz)

L: transmission loss = $L_b - G_t - G_r$

L_a: non-deviative and deviative absorption

L_b: basic transmission loss = $L_{bf} + L_a + L_c + L_h + L_m + L_q + L_r + L_z - G_f$

L_{bf}: basic free-space transmission loss = $32.4 + 20 \log f + L_f$

L_c: polarization-coupling loss and multiple-hop ground-reflection loss

L_d: spatial attenuation = $L_f - G_f$

L_f: free-space attenuation relative to a 1 km path

L_h: auroral absorption

L_m: loss associated with propagation at frequencies above the MUF

L_q: sporadic-E obscuration loss

L_r: sporadic-E reflection loss

L_{rc}: loss in receiving antenna circuit, excluding the loss associated with the antenna radiation resistance

L_s: system loss = $L + L_{tc} + L_{rc}$

L_{tc}: loss in transmitting antenna circuit, excluding the loss associated with the antenna radiation resistance

L_z: additional loss

G_f: focus gain

G_r: receiving antenna gain

G_t: transmitting antenna gain

Other symbols

δ: mean solar declination

Δ: elevation angle

θ: geographic longitude

λ: geographic latitude

Θ: angle between the direction of propagation and the Earth's magnetic field

θ_1: mean gradient of virtual height

φ: corrected geomagnetic latitude

χ: solar-zenith angle

f_v: frequency at virtual incidence

f_j: plasma frequency

f_{ob}: oblique incidence propagation

f_m: median mode MUF

F_u: ratio of the upper decile to the median MUF

F_l: ratio of the lower decile to the median MUF

h: true height of reflection at vertical incidence

h': virtual height of reflection at vertical incidence

h_j: height of intersection of the F1 and F2 of the model f_j

i: zenithal angle of the unrefracted oblique ray

I: magnetic dip

K: magnetic index

K_I: ionospheric and Earth-curvature correction term

O: ordinary wave

Q: mode availability (%)

R: Earth's radius

R_H: Fresnel-reflection coefficient for horizontal wave polarization

R_V: Fresnel-reflection coefficient for vertical wave polarization

T: universal time

t: local time

X: modified magnetic dip

X: extraordinary wave

1. Introduction

Question 30/6 draws attention to the continuing need for an internationally agreed method of estimating the field strength and transmission loss at frequencies above 1.6 MHz of signals which propagate via sky waves between ground-based terminals. Interim Working Party 6/1 (formerly known as International Working Party VI/1) has been established with terms of reference which are currently given in Decision 6-2. These terms include the development of both computer-based and manual prediction methods for such signals.

The fundamental difficulties of producing an accurate prediction method for the frequency range 1.6 to 2 MHz and the importance of ensuring that any such method is consistent with the method for the frequency range 150 to 1600 kHz which is given in Annex I to Recommendation 435-3, have been readily recognized; so the difficulties at frequencies above 30 MHz have also been appreciated, where the regularly refracted propagation modes usually cannot exist and the dominant signals travel via ground sidecatter or by scattering from sporadic-E irregularities or irregularities in the F-region of the ionosphere. Accordingly, the initial objectives of the Working Party were to develop a prediction method based on conventional propagation modes for the frequency range 2 to 30 MHz.

Consideration was given to various prediction methods in use in different countries [Barghausen *et al.*, 1969; Beckmann, 1967; Damboldt, 1976; Halley, 1965; Harnischmacher, 1960; Kasantsev, 1947, 1956, 1957; Laitinen and Haydon, 1950; Lucas and Haydon, 1966; Miya and Kanaya, 1955; NBS, 1948; Piggott, 1959; Rao, 1969 and Rawer, 1952]. By amalgamating different aspects from these, an interim method was produced. This was submitted to the CCIR and adopted as Report 252-2 (New Delhi, 1970).

Opinion 45 calls for evaluations of the accuracy of this first interim method and some comparisons with observational data are given in Report 571-1. The method has been found to be generally satisfactory, but it has a number of systematic shortcomings. With the present improved understanding of ionospheric and signal characteristics and in the light of experience gained in using the interim method, Interim Working Party 6/1 proposed to the XIIIth Plenary Assembly that a completely revised prediction method should be developed and presented to the next Interim Meeting of Study Group 6. Report 572 (Geneva, 1974) outlined the general procedures to be followed in this revision.

The present Report describes in detail the method that has been devised. It is based on CCIR texts and other documentation current as of March 1976 at the close of the Interim Meeting of Study Group 6. The associated computer program and explanatory documentation required for its use are being produced and made available for distribution separately.

It must be appreciated that the method, like its predecessor, is provisional in the sense that in due course it will probably be superseded by an improved method. However, this statement should not be interpreted as implying the current existence of evidence of inaccuracy.

2. Requirements for predictions

Field strength and transmission-loss predictions are needed as an aid to circuit planning, for frequency management and for subsequent investigations. The requirements in the three cases differ. For circuit planning, principal attention must be paid to median conditions, although some statistical consideration should also be given to day-to-day changes. The need is for so-called long-term predictions.

When predictions are employed for real-time frequency management, it is usual to attempt to update the long-term predictions in terms of some locally measured real-time parameter such as foF2 or magnetic *K*-index [Barghausen *et al.*, 1969]. For subsequent investigations, measured oblique or vertical-incidence ionograms may be available, leading to improved representations of the prevailing ionospheric conditions.

The prediction method described here is a long-term prediction method based entirely on past data. It yields values of the monthly medians of hourly smoothed sky-wave field strengths and transmission losses. It is intended that the method will be used in conjunction with a computer and that a simpler version for manual evaluations will be produced separately.

For the estimation of the signal quality to be expected in any communications circuit, signal-strength data alone are insufficient and must be supplemented by quantitative information about other parameters, especially noise, as available in Reports 322-1 and 258-3. A procedure for the prediction of a specified signal-to-noise ratio given by Barghausen *et al.* [1969] is available as an option.

3. Principles of the method

To appreciate the principles of the proposed method it is appropriate first to consider briefly the philosophy of prediction techniques in general. The ultimate objective is for a prediction method which is both accurate and simple. There are two different approaches which may be followed. One is to fit empirical equations to the dependence of measured transmission loss on path, time and frequency parameters. The other is to estimate the loss as the sum of a number of separate terms, each of which is given by an expression which has been deduced either from theory or from measurement. Both techniques have limitations. The former method is likely to be simpler but, unless it has been derived from a large data base, the observed trends may not be truly representative. The latter method is conceptually more elegant and enables variations to be specified in a physically meaningful manner. However, there remains the possibility of error due to failure to allow for an important term or to an inexact allowance. There is also a likelihood of devising a method which is over-complex and for which the accuracy achieved does not merit some of the complications that have been introduced.

It is clear that the optimum method for manual evaluations is likely to be less accurate than the optimum computer-based method, since some calculations which are appropriate for computer solution would be prohibitively lengthy. Nevertheless, despite the widespread availability of high-speed computers, it is important to ensure that, even for the computer-based method, all calculations are kept to a minimum. To some extent it is legitimate to initially introduce stages of calculation because of their physical justification, and then later to simplify these if it can be generally established that the accuracy of prediction has not been unacceptably reduced.

The method presented here assumes great-circle propagation with reflection from the E, F and sporadic-E layers. Although in principle it may be used for paths of any range, like its predecessor it is liable to be less accurate for ranges beyond 10 000 km. This is in part because for such long paths, and particularly those between near-antipodal terminals, in practice the azimuth of the dominant signals changes appreciably with temporal variations in maximum usable frequency and ionospheric absorption [Miya *et al.*, 1957; Miya and Kawai, 1959]. With regard to the fact that predictions for long ranges are also of great importance, more efforts should be made to improve the accuracy of the predictions for ranges beyond 10 000 km, even beyond 20 000 km [CCIR, 1970-74].

As with the method of Annex I to Recommendation 435-3 for MF, a combination of the separate-loss-term and empirical-equation procedures is proposed. The former procedure is to be used for wave frequencies below the standard maximum usable frequency or estimated junction frequency (EJF)—referred to sometimes simply as the MUF. At higher frequencies, where it is not possible to predict the existence of conventional modes yet, there is ample evidence that strong signals propagate; the method relies on empirical equations derived from an analysis of measured field-strength data. Account is taken of signals reflected from sporadic-E irregularities only at frequencies above the path MUF and provided the range is 4000 km or less. Estimated signal intensities given by the empirical equations for these frequencies are compared with the corresponding sporadic-E mode monthly median intensities and the greater values regarded as applying.

The separate-loss-term procedure consists of three main stages. Firstly, it is necessary to predict the state of the ionosphere—to produce a representation of the height distributions of electron concentration along the propagation path. Secondly, the ray paths of all propagation modes which can exist between transmitter and receiver must be determined. Then the transmission loss of each active mode is deduced in terms of the ray path directions. In deriving the overall transmission loss (see Recommendation 341), the transmitting and receiving antenna gains and terminal losses due to imperfect ground are taken into account. The signal strengths of the different modes are given in terms of the transmitter radiated power, and the available power from the receiving antenna is determined by summing the powers from the separate modes, on the assumption that these signal components have random relative phases.

The empirical expressions used for frequencies above the MUF have been chosen to ensure consistency of the estimated field strengths with values predicted by the separate-loss-term procedure at lower frequencies. They give a smooth decrease of field strength with increase of wave frequency at a rate which depends on the MUF and so is a function of time of day and season, level of solar activity, path geographical region and path length. Above the MUF the predictions should be regarded as applying to a composite mode, since it is not possible to specify by which propagation path the signals then travel.

The ionosphere is subject to systematic diurnal and seasonal changes, but it is usual to assume that variations which occur within an hour or from day-to-day within a month at a given hour are random. Accordingly, the predictions of field strength and transmission loss give representative monthly median values for each hour. Such predictions may be supplemented, as in the method to be described, by estimates of the likely fluctuations about these median values determined from ionospheric variability statistics. Fig. 1 lists the procedures given in Report 572 (Geneva, 1974) which the Interim Working Party 6/1 was instructed to consider in the formulation of the revised prediction method, and Fig. 2 is a simplified schematic representation of the stages of computation that are now proposed. These stages are described in detail in the later sections of this Report.

4. Ionospheric characteristics

4.1 *Monthly median values*

Propagation modes involving reflection from the E and the F-layers are determined using an ionospheric model which has parameters that vary over the great-circle path and are given in terms of the vertical-incidence ionospheric characteristics foF2, foE, M(3000)F2 and h'F,F2 [Piggott and Rawer, 1972]. (h'F,F2 is the minimum virtual height of signal reflection from the F2-layer. It is equal to h'F by night and to h'F2 when foF1 is observed by day.) The intensity of signals reflected from the sporadic-E layer is expressed as a function of appropriate values of the vertical-incidence ionospheric characteristic foEs.

The quantities foF2, foE, M(3000)F2, h'F, h'F2 and foEs are recorded from ionograms each hour of each day by a world network of ionosonde stations. From the monthly medians of past measured values, empirical equations have been produced to represent their geographical and temporal morphologies. The dependence on solar activity is expressed in terms of the twelve-month running mean sunspot number R_{12} (in the case of foF2, M(3000)F2, h'F,F2 and foEs) and the monthly mean 10.7 cm solar radio-noise flux Φ (in the case of foE). For prediction purposes it is appropriate to approximate Φ by an estimate of Φ_{12}, the twelve-monthly smoothed value. These empirical equations are then used to provide forecasts of the values of the ionospheric characteristics for a given sunspot number or solar flux. Although the relationship between the two solar indices varies for different solar cycles and for the upgoing and downcoming halves of a single cycle, the mean relationship between R_{12} and Φ_{12}, determined by Stewart and Leftin [1972] is taken. Hence, an estimate of either the sunspot number or the solar flux on its own may be used in the prediction system. Stewart and Leftin give

$$\Phi_{12} = 63.7 + 0.728\ R_{12} + 0.00089\ R_{12}^2 \tag{1}$$

and

$$R_{12} = \sqrt{95524 + 1123\ \Phi_{12}} - 408.8 \tag{2}$$

where Φ_{12} is expressed in units of $10^{-22}\ \mathrm{Wm^{-2}\ Hz^{-1}}$.

The equations which define foF2, M(3000)F2, h'F,F2 and foEs [Jones *et al.*, 1969] require sets of numerical coefficients for their evaluation, and details of these are given in Report 340-3. Coefficients are available for M(3000)F2 for each month for reference levels of low and high solar activity $R_{12} = 0$ and 100; coefficients for h'F,F2 [Leftin *et al.*, 1967] and of foEs [Leftin *et al.*, 1968] (for solar epochs corresponding to R_{12} approximately 10 and 180 for h'F,F2 and approximately 10 and 150 for foEs) are also available for each month. Values of the ionospheric characteristics for any general level of solar activity are determined by linear interpolation or extrapolation between the values deduced from the coefficients for these reference solar-activity levels.

In the case of foF2 there are two different sets of coefficients available, known respectively as the Oslo and New Delhi sets. The Oslo set has been produced in a similar way to that for M(3000)F2 with different coefficients for each month with $R_{12} = 0$ and 100. The New Delhi set [Jones and Obitts, 1970] is based on a single representation which gives smoothed mean values centred on any day of the year and for any solar activity. In particular, the dependence on solar index is non-linear and varies with position and time. Interim Working Party 6/3 is currently assessing the relative accuracies of these two representations and examining whether any reduced accuracy ensues from the combined use of values of foF2 based on a non-linear dependence on solar index with values of other ionospheric characteristics relying on a linear dependence. In advance of any conclusions from these investigations, the Oslo set of coefficients is used in the present prediction method. However, caution should be exercised for $R_{12} > 150$ because it is known (Report 340-3) that saturation effects arise at some locations and times.

Each ionospheric characteristic is represented for a given month and solar activity by orthogonal-polynomial expressions in terms of geographic latitude λ, geographic longitude θ and Universal Time T. The general characteristic $\Omega\ (\lambda, \theta, T)$ is expressed as a time series:

$$\Omega\ (\lambda, \theta, T) = \sum_j [a_j\ (\lambda, \theta)\ \cos\ jT + b_j\ (\lambda, \theta)\ \sin\ jT] \tag{3}$$

where a and b give the latitude and longitude variations, being defined as:

$$a_j\ (\lambda, \theta) = \sum_k U_{2j,k} \times G_k\ (\lambda, \theta)$$

$$b_j\ (\lambda, \theta) = \sum_k U_{2j-1,k} \times G_k\ (\lambda, \theta) \tag{4}$$

U is numerical coefficient and G is trigonometric function of latitude, longitude, and modified magnetic dip X. X is a combined geographic and magnetic parameter defined as

$$X = \text{arc tan}\left[\frac{I}{\sqrt{\cos \lambda}}\right] \tag{5}$$

where I is the magnetic dip (in radians, considered positive if north of the magnetic equator) taken from the spherical-harmonic analysis model of the Earth's magnetic field produced for epoch 1960 by Jensen and Cain [1962]. X is positive in the Northern hemisphere. The number of terms in the above summations varies for the different characteristics, depending on the amount of variation of the given characteristic.

Monthly median foE is given by empirical equations derived by Muggleton [1975] from an analysis of published data for the years 1944-1973 from 55 ionospheric stations. (See also Report 340-2. It is to be noted that Report 340-3 contains revisions not taken into account because, as already stated, the method is based on documentation current as of March 1976.)

$$\text{foE} = \left[(1 + 0.0094\,[\Phi_{12} - 66])\cos^{m}\chi_{noon}\,(A + B\cos\lambda)\,D\right]^{0.25} \tag{6}$$

where Φ_{12} is expressed in units of $10^{-22}\,\text{Wm}^{-2}\,\text{Hz}^{-1}$.

χ_{noon} = solar-zenith angle at local noon

and λ = geographic latitude, considered positive if north of the equator.

$$\begin{aligned}&\text{For } |\lambda| < 32^\circ \; m = -1.93 + 1.92\cos\lambda;\; A = 23 \text{ and } B = 116\\ &\text{For } |\lambda| \geqslant 32^\circ \; m = 0.11 - 0.49\cos\lambda;\; A = 92 \text{ and } B = 35\end{aligned} \tag{7}$$

D is the time-of-day factor, given as follows:

(a) for $\chi' \leqslant 73^\circ$

$$D = \cos^{p}\chi' \tag{8a}$$

where χ' is related to the solar-zenith angle χ. For $|\lambda| \leqslant 23^\circ$ $\chi' = \chi$, but for $|\lambda| > 23^\circ$, χ' is taken to be the value of χ at a time 0.05 hours earlier. This correction allows for the "sluggish" nature of the ionosphere. For $|\lambda| \leqslant 12^\circ$, $p = 1.31$; for $|\lambda| > 12^\circ$, $p = 1.20$;

(b) for $73^\circ < \chi' < 90^\circ$

$$D = \cos^{p}(\chi' - \delta\chi') \tag{8b}$$

$$\text{where} \quad \delta\chi' = 6.27 \times 10^{-13}(\chi' - 50)^{8} \quad \text{degrees} \tag{8c}$$

with χ' in degrees, and p is as in (a) above;

(c) for $\chi' \geqslant 90^\circ$

$$D = (0.077)^{p}\exp\,[-1.68\,(t_1 - t)] \quad \text{from midnight to dawn} \tag{8d}$$

$$\text{and} \quad D = (0.077)^{p}\exp\,[-1.01\,(t - t_2)] \quad \text{from sunset to midnight} \tag{8e}$$

where t is the local time of interest in hours,

t_1 is the local time at dawn ($\chi' = 90^\circ$) in hours,

t_2 is the local time at sunset ($\chi' = 90^\circ$) in hours,

p has the same value as in (a) above,

foE is taken as having a minimum value, following Wakai [1971] of

$$\text{foE} = \left[0.017\,(1 + 0.0098\,R_{12})^{2}\right]^{0.25} \tag{9}$$

4.2 *Day-to-day scatter statistics and mode availability*

Estimates of the mode availability, which is the probability that an oblique sky-wave path which has been deduced using monthly median values of the ionospheric characteristics will exist on a given day, may be derived in terms of the statistics of the day-to-day variations of the mode MUF. It is assumed after Zacharisen and Crow [1970] that MUF variations follow a χ^2-distribution so that equations developed by Bradley and Bedford [1976], which approximate to that distribution, apply.

The mode availability Q expressed as a percentage is given in terms of f, the wave frequency, and f_m, the median mode MUF, by:

– for $f \leqslant f_m$

$$Q = 130 - \frac{80}{1 + \left(\frac{1 - \frac{f}{f_m}}{1 - F_l}\right)} \tag{10a}$$

or 100, whichever is the smaller;

– for $f > f_m$

$$Q = \frac{80}{1 + \left(\frac{\frac{f}{f_m} - 1}{F_u - 1}\right)} - 30 \tag{10b}$$

or 0, whichever is the larger.

F_u is the ratio of the upper decile to the median MUF and F_l is the ratio of the lower decile to the median.

The determination of the median MUF is discussed in § 6.2. F_u and F_l are found as follows:

(*a*) *E-modes*

foE is relatively constant from day-to-day; Rush and Gibbs [1973] have shown that the day-to-day fractional variability of foE about the median value is only a factor of 0.3 to 0.5 of that of foF2. Nevertheless, foE variations provide the principal contribution to day-to-day changes in the MUF of E-modes since ray reflection heights are almost constant. Analyses by Tiffon [1974] of a selection of low and middle-latitude foE data are consistent with adopting fixed values of $F_u = 1.05$ and $F_l = 0.95$ for all locations and times. Hence, these values are taken as applying to the MUF for both single and multiple-hop modes.

(*b*) *F-modes*

King and Slater [1973] have shown that the relative day-to-day variability of M(3000)F2 is appreciably less than that of foF2. Rush *et al.* [1974] have considered the implications of this feature to oblique HF communication paths and concluded that, although F-layer heights are more variable than those of the E and Es-layers, it is still justifiable for single-hop modes to take the fractional MUF variability as independent of path range. Barghausen *et al.* [1969] have reported an analysis of the variability of foF2 and M(3000)F2 for 13 well-distributed ionosonde stations; they gave variability parameters of MUF(3000)F2 for different times and geographical regions. Table I, taken from their results, lists F_u and F_l for different seasons, ranges of R_{12}, midpath local times and midpath geographic latitudes. It is possible that multiple-hop modes over long paths may be subject to greater day-to-day variations than short single-hop modes because ionospheric variability is uncorrelated on the different hops; however, in the absence of more precise information, the values of Table I are taken as applying to the MUF for any transmission range. These F-layer values are also used in the case of multiple-order modes with successive reflection from the E- and F-layers. In the case of reflection from the sporadic-E layer monthly median signal intensities are determined in accordance with the procedure described in § 7.5.2 as a function of monthly median foEs and these components are taken as having an availability of 50%.

TABLE IA – *MUF variability parameters F_u and F_l of F-modes for R_{12} less than 50 as a function of season, midpath local time t and midpath geographic latitude λ (N or S of equator)*

		$R_{12} < 50$												
λ \ t		22-02		02-06		06-10		10-14		14-18		18-22		
		F_u	F_l	F_u	F_l	F_u	F_l	F_u	F_l	F_u	F_l	F_u	F_l	
>75°		1.44	0.60	1.34	0.65	1.45	0.69	1.32	0.72	1.33	0.68	1.40	0.67	Winter
65-75°		1.37	0.68	1.29	0.71	1.38	0.75	1.23	0.76	1.24	0.75	1.35	0.70	
55-65°		1.30	0.74	1.24	0.76	1.27	0.80	1.15	0.80	1.17	0.82	1.30	0.73	
45-55°		1.25	0.79	1.21	0.78	1.16	0.83	1.12	0.85	1.12	0.84	1.25	0.76	
35-45°		1.23	0.81	1.20	0.79	1.13	0.85	1.11	0.87	1.11	0.89	1.23	0.77	
25-35°		1.28	0.81	1.30	0.74	1.15	0.86	1.17	0.82	1.15	0.85	1.28	0.78	
15-25°		1.34	0.78	1.37	0.67	1.19	0.87	1.20	0.75	1.24	0.77	1.32	0.79	
<15°		1.27	0.71	1.38	0.70	1.18	0.88	1.15	0.86	1.14	0.87	1.20	0.79	
>75°		1.42	0.67	1.32	0.72	1.29	0.74	1.26	0.73	1.33	0.80	1.48	0.65	Equinox
65-75°		1.38	0.70	1.25	0.75	1.25	0.76	1.23	0.74	1.26	0.82	1.40	0.69	
55-65°		1.32	0.73	1.21	0.78	1.22	0.80	1.20	0.75	1.20	0.81	1.31	0.73	
45-55°		1.26	0.75	1.19	0.80	1.20	0.81	1.18	0.76	1.16	0.81	1.26	0.76	
35-45°		1.22	0.77	1.20	0.81	1.19	0.81	1.16	0.77	1.16	0.80	1.25	0.78	
25-35°		1.22	0.78	1.26	0.80	1.18	0.82	1.15	0.78	1.16	0.81	1.28	0.74	
15-25°		1.30	0.77	1.32	0.75	1.16	0.83	1.14	0.81	1.18	0.83	1.33	0.69	
<15°		1.23	0.76	1.40	0.66	1.13	0.86	1.13	0.89	1.19	0.86	1.16	0.75	
>75°		1.26	0.68	1.24	0.79	1.15	0.84	1.17	0.87	1.21	0.85	1.22	0.76	Summer
65-75°		1.22	0.70	1.18	0.81	1.14	0.83	1.15	0.86	1.16	0.86	1.18	0.77	
55-65°		1.18	0.72	1.17	0.84	1.14	0.83	1.15	0.84	1.14	0.86	1.15	0.81	
45-55°		1.17	0.75	1.20	0.85	1.15	0.82	1.16	0.83	1.14	0.85	1.15	0.84	
35-45°		1.17	0.79	1.25	0.85	1.17	0.80	1.17	0.82	1.15	0.83	1.16	0.85	
25-35°		1.18	0.79	1.30	0.82	1.17	0.78	1.20	0.80	1.19	0.81	1.20	0.80	
15-25°		1.20	0.77	1.34	0.78	1.14	0.77	1.24	0.79	1.22	0.79	1.23	0.73	
<15°		1.20	0.74	1.37	0.75	1.12	0.80	1.30	0.83	1.27	0.82	1.20	0.69	

Winter : Nov, Dec, Jan, Feb in the N. hemisphere and May, Jun, Jul, Aug in the S. hemisphere.
Summer : May, Jun, Jul, Aug in the N. hemisphere and Nov, Dec, Jan, Feb in the S. hemisphere.
Equinox : Mar, Apr, Sep, Oct in both hemispheres.

TABLE IB – *MUF variability parameters F_u and F_l of F-modes for R_{12} greater than or equal to 50 and less than or equal to 100 as a function of season, midpath local time t and midpath geographic latitude λ (N or S of equator)*

λ \ t	$50 < R_{12} < 100$												
	22-02		02-06		06-10		10-14		14-18		18-22		
	F_u	F_l	F_u	F_l	F_u	F_l	F_u	F_l	F_u	F_l	F_u	F_l	
≥75°	1.45	0.76	1.39	0.78	1.44	0.68	1.40	0.67	1.33	0.62	1.45	0.70	
65-75°	1.39	0.79	1.31	0.81	1.37	0.74	1.32	0.70	1.29	0.73	1.41	0.73	
55-65°	1.33	0.82	1.24	0.83	1.25	0.79	1.21	0.75	1.22	0.80	1.33	0.76	
45-55°	1.30	0.84	1.19	0.82	1.14	0.83	1.15	0.81	1.16	0.84	1.29	0.78	Winter
35-45°	1.27	0.83	1.17	0.81	1.12	0.85	1.14	0.86	1.14	0.86	1.28	0.79	
25-35°	1.30	0.78	1.31	0.76	1.16	0.85	1.18	0.85	1.18	0.85	1.32	0.78	
15-25°	1.33	0.74	1.38	0.71	1.17	0.85	1.22	0.83	1.26	0.82	1.40	0.76	
<15°	1.21	0.77	1.26	0.69	1.14	0.87	1.13	0.86	1.15	0.85	1.23	0.78	
≥75°	1.45	0.64	1.31	0.61	1.27	0.73	1.28	0.74	1.30	0.74	1.47	0.67	
65-75°	1.41	0.68	1.22	0.71	1.23	0.77	1.26	0.74	1.26	0.78	1.38	0.70	
55-65°	1.35	0.70	1.17	0.75	1.20	0.80	1.23	0.72	1.18	0.78	1.29	0.73	
45-55°	1.28	0.73	1.15	0.77	1.17	0.81	1.21	0.74	1.13	0.76	1.20	0.75	
35-45°	1.22	0.75	1.16	0.78	1.16	0.82	1.18	0.78	1.12	0.76	1.17	0.76	Equinox
25-35°	1.22	0.77	1.22	0.76	1.15	0.82	1.17	0.83	1.14	0.78	1.23	0.72	
15-25°	1.32	0.75	1.30	0.73	1.13	0.84	1.15	0.87	1.17	0.81	1.37	0.69	
<15°	1.18	0.79	1.39	0.68	1.11	0.86	1.13	0.89	1.20	0.84	1.23	0.80	
≥75°	1.27	0.82	1.23	0.80	1.20	0.82	1.18	0.85	1.24	0.80	1.23	0.79	
65-75°	1.23	0.83	1.19	0.82	1.19	0.79	1.17	0.82	1.17	0.82	1.19	0.82	
55-65°	1.20	0.83	1.18	0.82	1.19	0.77	1.17	0.79	1.14	0.82	1.17	0.83	
45-55°	1.17	0.81	1.19	0.81	1.21	0.76	1.17	0.77	1.15	0.81	1.16	0.82	Summer
35-45°	1.17	0.78	1.22	0.78	1.23	0.75	1.18	0.78	1.17	0.78	1.17	0.78	
25-35°	1.20	0.77	1.30	0.83	1.22	0.75	1.19	0.79	1.19	0.77	1.18	0.74	
15-25°	1.26	0.77	1.38	0.69	1.17	0.78	1.23	0.82	1.23	0.78	1.28	0.73	
<15°	1.26	0.79	1.44	0.63	1.11	0.84	1.28	0.85	1.28	0.81	1.22	0.77	

Winter : Nov, Dec, Jan, Feb in the N. hemisphere and May, Jun, Jul, Aug in the S. hemisphere.
Summer : May, Jun, Jul, Aug in the N. hemisphere and Nov. Dec. Jan, Feb in the S. hemisphere.
Equinox : Mar, Apr, Sep, Oct in both hemispheres.

TABLE IC – *MUF variability parameters F_u and F_l of F-modes for R_{12} greater than 100 as a function of season, midpath local time t and midpath geographic latitude λ (N or S of equator)*

λ \ t	$R_{12} > 100$												
	22-02		02-06		06-10		10-14		14-18		18-22		
	F_u	F_l	F_u	F_l	F_u	F_l	F_u	F_l	F_u	F_l	F_u	F_l	
≥75°	1.36	0.62	1.27	0.70	1.41	0.74	1.42	0.67	1.40	0.64	1.43	0.73	
65-75°	1.31	0.69	1.25	0.74	1.34	0.77	1.30	0.72	1.16	0.72	1.34	0.78	
55-65°	1.26	0.77	1.23	0.78	1.24	0.81	1.18	0.80	1.11	0.79	1.26	0.82	
45-55°	1.19	0.83	1.19	0.80	1.16	0.84	1.11	0.87	1.09	0.84	1.20	0.86	
35-45°	1.15	0.86	1.14	0.81	1.13	0.87	1.09	0.90	1.09	0.87	1.14	0.87	Winter
25-35°	1.22	0.83	1.26	0.76	1.12	0.89	1.09	0.90	1.11	0.88	1.13	0.86	
15-25°	1.32	0.78	1.35	0.70	1.12	0.89	1.12	0.89	1.14	0.89	1.20	0.83	
≤15°	1.18	0.83	1.25	0.76	1.14	0.89	1.13	0.90	1.15	0.89	1.20	0.84	
≥75°	1.46	0.66	1.37	0.67	1.35	0.75	1.40	0.66	1.38	0.70	1.46	0.72	
65-75°	1.42	0.67	1.31	0.71	1.30	0.73	1.31	0.70	1.33	0.70	1.37	0.72	
55-65°	1.30	0.69	1.25	0.75	1.27	0.71	1.24	0.71	1.25	0.71	1.24	0.72	
45-55°	1.18	0.73	1.20	0.78	1.25	0.70	1.20	0.72	1.16	0.74	1.17	0.73	
35-45°	1.15	0.79	1.16	0.82	1.17	0.75	1.16	0.78	1.12	0.80	1.14	0.84	
25-35°	1.25	0.81	1.18	0.82	1.10	0.87	1.10	0.87	1.11	0.87	1.15	0.86	
15-25°	1.31	0.81	1.32	0.77	1.11	0.89	1.11	0.92	1.12	0.90	1.20	0.85	
≤15°	1.21	0.80	1.23	0.79	1.09	0.86	1.20	0.90	1.14	0.90	1.23	0.82	Equinox
≥75°	1.30	0.73	1.27	0.74	1.17	0.82	1.15	0.83	1.23	0.79	1.24	0.75	
65-75°	1.22	0.75	1.22	0.75	1.20	0.77	1.18	0.80	1.21	0.80	1.23	0.77	
55-65°	1.16	0.77	1.18	0.76	1.26	0.74	1.21	0.77	1.19	0.80	1.21	0.80	
45-55°	1.14	0.79	1.15	0.76	1.30	0.73	1.26	0.75	1.19	0.80	1.18	0.84	
35-45°	1.14	0.80	1.14	0.76	1.30	0.75	1.27	0.75	1.19	0.79	1.16	0.84	
25-35°	1.16	0.81	1.15	0.76	1.25	0.82	1.20	0.81	1.17	0.79	1.15	0.83	
15-25°	1.21	0.81	1.22	0.77	1.18	0.85	1.15	0.86	1.18	0.81	1.19	0.80	
≤15°	1.25	0.80	1.21	0.79	1.13	0.86	1.17	0.89	1.22	0.85	1.23	0.78	Summer

Winter : Nov, Dec, Jan, Feb in the N. hemisphere and May, Jun, Jul, Aug in the S. hemisphere.
Summer : May, Jun, Jul, Aug in the N. hemisphere and Nov, Dec, Jan, Feb in the S. hemisphere.
Equinox : Mar, Apr, Sept, Oct in both hemispheres.

5. Models of vertical distributions of electron concentration

It was noted in § 4.1 that propagation modes involving reflection from the E and F-layers are determined using an ionospheric model with parameters which depend on foF2, foE, M(3000)F2 and h'F,F2. This model is given in Report 340-3 and is illustrated in Fig. 3. It consists of:

— a parabolic E-layer below its height of maximum electron concentration hmE, with semi-thickness ymE. hmE is taken as constant at 110 km and ymE as 20 km. These values have been chosen as generally consistent with available measured data [Maeda, 1969; 1971];

— a parabolic F2-layer with height of maximum electron concentration hmF2 and semi-thickness ymF2;

— a linear increase of electron concentration with height between hmE and the point on the parabolic F2-layer where the plasma frequency f_j is 1.7 foE.

The model parameters hmF2 and ymF2 are given from the empirical equations [Bradley and Dudeney, 1973; Eyfrig, 1974]:

$$\text{hmF2} = \frac{1490}{\text{M(3000)F2} + \Delta M} - 176 \tag{11a}$$

$$\text{with } \Delta M = \frac{0.18}{x - 1.4} + \frac{0.096\,(R_{12} - 25)}{150} \tag{11b}$$

where $x = \dfrac{\text{foF2}}{\text{foE}}$ or 1.7, whichever is the larger.

$$\text{ymF2} = \text{hmF2} - \text{h'F, F2} + \Delta h' \tag{12a}$$

where

$$\Delta h' = \left(\frac{0.613}{x - 1.33}\right)^{0.86} \times (\text{hmF2} - 104) \tag{12b}$$

ymF2 has a pre-set minimum value of 35 km and a maximum value of (hmF2 – hmE).

For the special case when $x = 1.7$ the electron concentration is taken as increasing linearly with height between hmE and hmF2

$$\text{i.e. ymF2} = 0 \text{ for } x = 1.7 \tag{12c}$$

In particular, no Fl-layer characteristics are used in formulating the model and the ionisation in the Fl-height region is taken as being given entirely in terms of the E- and F2-layer ionisation parameters. Measured true-height profiles rarely show marked Fl-layer discontinuities and many of the inflexions and cusps interpreted on ionograms as Fl-layer characteristics result from only minor fluctuations in electron concentration. The model has advantages over other models based on foFl in that there is no abrupt change when that parameter ceases to be observed.

Comparisons with true-height analyses of sample ionograms recorded at different locations, times of day, season and solar epoch confirm that the model estimates, based on measured values of vertical-incidence ionospheric characteristics, of the heights corresponding to given electron concentrations are usually correct to within 20 to 30 km.

Figure 4a is an example showing an ionogram recorded at Argentine Islands at 1645 local time (LT) on 29 September 1958. The corresponding height distributions of electron concentration deduced from true-height analysis may be compared with those given by the model using equations (11) and (12) and the observed values of the appropriate ionospheric characteristics (see Fig. 4b).

The method of determination of oblique ray paths described in § 6 requires a knowledge of the true and virtual heights of reflection at vertical incidence, h and h', of waves of specified frequency. For different ranges of frequency f_v, the following equations apply:

– for $f_v \leqslant \text{foE}$ with $\dfrac{f_v}{\text{foE}} = x_E$

$$h = \text{hmE} - \text{ymE}\sqrt{1 - x_E^2} \tag{13}$$

$$h' = (\text{hmE} - \text{ymE}) + x_E \times \text{ymE} \times \text{arc tanh } x_E \tag{14}$$

– for $\text{foE} < f_v \leqslant f_j$ with $\dfrac{f_v}{f_j} = x_j;\ x_E \geqslant 1$

$$h = \text{hmE} + (h_j - \text{hmE})\ \frac{x_j^2\,(x_E^2 - 1)}{(x_E^2 - x_j^2)} \tag{15}$$

$$h' = (\text{hmE} - \text{ymE}) + x_E \times \text{ymE} \times \text{arc coth}\ x_E + 2\,(h_j - \text{hmE}) \times \frac{x_j^2\ x_E\ \sqrt{x_E^2 - 1}}{(x_E^2 - x_j^2)} \tag{16}$$

– for $f_j < f_v \leqslant \text{foF2}$ with $\dfrac{f_v}{\text{foF2}} = x_{F2};\ x_E > 1;\ x_j > 1$

$$h = \text{hmF2} - \text{ymF2}\ \sqrt{1 - x_{F2}^2} \tag{17}$$

$$h' = (\text{hmE} - \text{ymE}) + x_E \times \text{ymE} \times \text{arc coth}\ x_E + 2\,(h_j - \text{hmE}) \times \times \frac{x_j\ x_E\left[x_j\ \sqrt{x_E^2 - 1} - x_E\ \sqrt{x_j^2 - 1}\right]}{(x_E^2 - x_j^2)} + x_{F2} \times \text{ymF2} \times \text{arc cosh}\left(\frac{\text{hmF2} - h_j}{\text{ymF2}\ \sqrt{1 - x_{F2}^2}}\right) \tag{18}$$

h_j is the height of intersection of the F1 and F2 portions of the model corresponding to the plasma frequency f_j. It is given by

$$h_j = \text{hmF2} - \text{ymF2}\ \sqrt{1 - \left(\frac{f_j}{\text{foF2}}\right)^2} \tag{19}$$

One minor limitation of the model that can be seen from the measured ionogram of Fig. 4a is that when a synthesized ionogram is produced using equations (13) to (19), this shows a spurious cusp at the frequency f_j which is associated with the gradient discontinuity between the linear and parabolic F-region segments of the model. Tests have shown that the associated errors in h' for neighbouring values of f_v may be considerably reduced in general by linear interpolation between the values of h' for $f_v = 1.5$ foE and 1.9 foE i.e. for $1.5\ \text{foE} < f_v < 1.9\ \text{foE} < \text{foF2}$

$$h'(f_v) = h'(1.5\ \text{foE}) + \frac{f_v - 1.5\ \text{foE}}{0.4\ \text{foE}}\left[h'(1.9\ \text{foE}) - h'(1.5\ \text{foE})\right] \tag{20}$$

The change this makes to the synthesized ionogram is seen in Fig. 4a. Equation (20) is used in the prediction method. In cases where

$$\frac{\text{foF2}}{\text{foE}} < 1.9$$

it cannot be applied, but virtual heights for $f_v \sim f_j$ are then large because of the closeness to foF2, so that errors become relatively small.

6 Sky-wave paths in the ionosphere

6.1 *Possible propagation modes*

Seven ray paths are evaluated which must be physically possible and must have elevation angles exceeding a minimum specified value. The sky-wave paths evaluated are: two ray paths via reflections from the regular E-layer, three ray paths via reflections from the F-layer; and two mixed modes.

The E-layer modes considered are, first, the mode with the least number of hops possible for the given elevation angle and, second, the mode with the next greater number of hops. The F-layer modes considered are, first, that with the least possible number of hops and then those two with successively greater numbers of hops. Sporadic-E layer refraction is ignored in relation to F-layer ray paths.

The mixed modes are considered only for paths longer than 3000 km and consist of one E-layer reflection, and one or more F-layer reflections. The first mixed mode consists of the 1E-hop and the remainder of the path by the least possible number of F-layer reflections. The second mixed mode is similar, but for the next greater number of F hops. The E- and F-layer hops may arise in any order.

For frequencies greater than the path MUF the dominant signals may be propagated by means of a single reflection from the Es-layer for transmission ranges of 2600 km and less and via two Es hops for transmission ranges of 2600 to 4000 km. The signal strenghts for these modes are determined as indicated in § 7.5.2.

6.2 *Determination of the MUF*

A knowledge of the MUF is needed to determine mode availability and for the empirical equations for signal strengths at the higher frequencies. Two separate procedures of MUF evaluation are available. In the one, ray computations are made for a succession of increasing frequencies until no propagation path to the desired transmission range is possible. Frequency increments of 0.5 MHz should provide values of adequate accuracy. Alternatively, use can be made of equations based on relationships for a mean reference ionosphere as given in Report 340-3. These express the MUF for an E-mode over the path in terms of foE and they express the MUF for an F2-mode in terms of foF2 and M(3000)F2.

For MUF computations the path is divided into portions depending on its length, so that a single E-hop does not exceed a ground range of 2500 km and a single F-hop does not exceed a range of 5000 km. The evaluation is undertaken at a reflection point for which foF2 is a minimum.

In the case of sporadic-E modes, no attempt is made to determine a MUF since it is believed that a realistic physical model consists of a gradually reducing number of irregularities which can provide reflection as the wave frequency is increased. This means that the effectiveness of these modes is governed entirely by signal-strength considerations.

6.3 *Reflection from the E and F-layers*

The determination of the active modes and their elevation angles is based on a representation of the ray paths by undeviated propagation between the ground and mirror-reflecting points in the ionosphere. The heights of the mirroring points are taken as the virtual heights of reflection of waves of "equivalent" frequency at vertical incidence. As already noted, great-circle propagation is assumed. The option is provided of incorporating longitudinal mirror tilts deduced from the predicted ionisation gradients. At very low elevation angles and appropriate tilt angles it may happen that a ray does not return to the Earth's surface, thus initiating a propagation mode of successive ionospheric reflections without intermediate ground reflections, as described in Report 250-4. This possibility is not yet considered in the prediction programme.

Ionospheric models are generated iteratively to correspond to the mirroring locations, and transmitter elevation angles are successively adjusted to ensure transmission to the desired ground range. The layer reflecting each active mode is readily given from the ratio of the equivalent vertical-incidence frequency to foE.

Consider a ray launched with elevation angle Δ_1 as indicated in Fig. 5. Suppose that reflection takes place from a plane reflector at range x_1 and of height h_{r1}, tilted through an angle ε_1 in the sense shown. Further, let the ray return to ground with elevation angle Δ_2 at range d_1. Then, if R is the Earth's radius:

$$\Delta_2 = \Delta_1 - 2\varepsilon_1 + \frac{(2x_1 - d_1)}{R} \tag{21}$$

$$x_1 = R\left[\text{arc cos}\left(\frac{R}{R + h_{r1}}\cos\Delta_1\right) - \Delta_1\right] \tag{22}$$

and

$$d_1 = 2x_1 + R\left[\Delta_1 - 2\varepsilon_1 - \text{arc cos}\left(\frac{R + h_{r1}}{R} \times \cos\left[\Delta_1 - 2\varepsilon_1 + \frac{x_1}{R}\right]\right)\right] \tag{23}$$

Hence, with Δ_1, ε_1 and h_{r1} given, x_1 and d_1 can be determined. For oblique-incidence propagation at a frequency f_{ob}, an "equivalent" vertical-incidence frequency f_{v1} is defined, such that h_{r1} may be taken as

$$h_{r1} = h'(f_{v1}) \tag{24}$$

where $h'(f_{v1})$ is the virtual height of reflection at vertical-incidence at frequency f_{v1}, as given for the ionospheric model by equations (14), (16), (18) and (20) as appropriate. f_{v1} is derived in terms of f_{ob} by

$$f_{v1} = f_{ob} \times K_1 \times \cos i_1 \tag{25}$$

where i_1 is the angle between the upgoing ray and the vertical at height h_{r1}. The angle i_1 is expressed in terms of x_1 and Δ_1 by:

$$i_1 = \frac{\pi}{2} - \left(\Delta_1 + \frac{x_1}{R}\right) \tag{26}$$

K_1 is an ionosphere and Earth-curvature correction term. It is determined by the approximate empirical expression [Bradley and Murphy, 1974]:

$$K_1 = \left(1 - \frac{1.5\,[h'(f_{v1}) - h(f_{v1})]}{R} \tan^2 i_1\right)^{\frac{1}{2}} \tag{27}$$

where $h(f_{v1})$ is the true height of reflection at vertical incidence at frequency f_{v1}, given for the ionospheric model by equations (13), (15) and (17) as appropriate. ε_1 is determined from the change in virtual height of reflection at frequency f_{v1} for the model ionospheres on either side of the reflection point along the great-circle path. With θ_1 defined as the mean gradient of virtual height over ranges of ± 200 km relative to the reflection position, appropriate distances for the scale size of the ionospheric mapping representation, then

$$\theta_1 = \frac{h'_{+200} - h'_{-200}}{400} \quad \text{radians} \tag{28}$$

After Titheridge [1958] ε_1 is taken as

$$\varepsilon_1 = \frac{\theta_1}{3} \tag{29}$$

The stages of analysis based on the above equations for the determination of the separate elevation angles on the successive hops of an n-hop mode propagated to a given ground range D are listed below.

Stage 1

Initially, it is supposed that there are no tilts and that all hops with reflection from the same layer have equal length. In the case of modes involving reflection from both the E- and F-layers, the E-layer hops are taken as having one third the ground-range span of the F-layer hops. For an assumed first-hop E-mode a first estimate of h_{r1} is hoE, the base height of the E-layer, and for an F-mode it is given as h'(0.95 foF2), as derived from the model ionosphere equations for the midhop position. These values lead to a first estimate of Δ_1 from:

$$\Delta_1 = \text{arc tan}\left(\cot\frac{d_1}{2R} - \frac{R}{R + h_{r1}}\,\text{cosec}\,\frac{d_1}{2R}\right) \tag{30}$$

where

$$d_1 = \frac{D}{n}$$

With Δ_1 known, i_1 is determined from equation (26) and initially taking $K_1 = 1$ leads to a first estimate of f_{v1} from equation (25).

Stage 2

Values of $h(f_{v1})$ and $h'(f_{v1})$ given by the model ionosphere equations for the mid-hop position are substituted in equation (27) to give an improved estimate of K_1, which in turn from equation (25) leads to an improved estimate of f_{v1}. This process is repeated a further twice, leading to an accurate value of h_{r1} from equation (24). The new h_{r1} is then substituted in equation (22) to give a better estimate of x_1 for which a new ionospheric model is generated.

Stages 3 and 4

The complete cycle of stages is repeated twice, leading to fourth estimates of x_1 and h_{r1}. Tests show these to be good approximations to the true mirror-reflecting ray apogee position.

Stage 5

ε_1, Δ_2 and a second estimate of d_1 are then computed from equations (28) and (29), (21) and (23) respectively.

Stage 6

With this Δ_2, the stages of calculation are repeated for subsequent hops of an n-hop mode, leading to corresponding elevation angles Δ_r and ground ranges d_r for all r up to $r = n$. First estimates of the rth hop parameters are taken as:

$$\Delta_r = \Delta_{r-1} - 2\varepsilon_{r-1} + \frac{2x_{r-1} - d_{r-1}}{R}$$

h_{tr}: final estimate of $h_{t(r-1)}$

$$x_r = R\left[\text{arc cos}\left(\frac{R}{R + h_{tr}}\cos\Delta_r\right) - \Delta_r\right]$$

$$i_r = \frac{\pi}{2} - \left(\Delta_r + \frac{x_r}{R}\right)$$

$$K_r = 1$$

$$f_{vr} = f_{ob} \times K_r \times \cos i_r \tag{31}$$

The total ground range for the n-hop mode launched with elevation angle Δ_1 is then

$$d = \sum_n d_1$$

whereas the required ground range is D.

Stages 7 and 8

To obtain a better estimate of Δ_1 (and hence of Δ_r) all calculations are repeated a maximum of a further four times using d'_1 as an improved estimate of d_1, where

$$d'_1 = d_1 + \left(\frac{D - \sum_n d_i}{n}\right) \tag{32}$$

The calculations are stopped for $|D - d| < 10$ km, and if this condition is not met by the fifth estimate of d, the mode is judged not to exist. Usually three or fewer estimates of Δ_1 are sufficient and it is only on the longer paths that five estimates are needed to give the desired ground range. When however the mode does exist, the procedure gives the elevation angles on the separate hops.

6.4 *Reflection from and transmission through the sporadic-E layer*

It has been noted in § 6.1 that although the sporadic-E layer undoubtedly sometimes prevents signals from penetrating to the F-layer, this blanketing effect is not directly taken into account. In determining the ray paths of F-modes, refraction in the Es-layer is likewise ignored.

Signals reflected from the Es-layer are assumed to have triangular ray paths equivalent to mirror reflection from a fixed height of 110 km. Hence the elevation angle Δ is readily given in terms of hop length d, by

$$\Delta = \text{arc tan}\left(\cot\frac{d}{2R} - \frac{R}{R + 110}\,\text{cosec}\,\frac{d}{2R}\right) \tag{33}$$

where R is the Earth's radius in kilometres.

6.5 *Frequencies above the MUF*

For frequencies above the MUF of all the possible modes considered in § 6.1, transmission is assumed to take place with reflection from the sporadic-E layer or via the mode with the greatest MUF. Ray path elevation angles are assumed to be those at the MUF. The transmission loss is given as that at the MUF, together with an additional loss term which increases rapidly with increase in frequency.

7. Transmission loss and gain factors

The separate transmission loss and gain factors which are specifically taken into account consist of:

— the transmitting and receiving-antenna gains;

— spatial attenuation, including focussing of rays with low elevation angles and rays propagated to very long distances;

— non-deviative, deviative and auroral absorption;

— polarization-coupling losses;

— multiple-hop ground-reflection losses;

— sporadic-E obscuration and reflection losses, and
— losses associated with propagation above the MUF.

Each of these factors can be large in some circumstances.

7.1 *Transmitting and receiving-antenna gains; G_t, G_r*

Transmission loss is markedly influenced by antenna beam directions and beamwidths, and the transmitting and receiving-antenna gains along the ray path directions, G_t and G_r respectively, are important terms in the overall prediction. It is unfortunate that the performance of a typical antenna sometimes departs appreciably from theory because of features such as local obstructions like nearby hills, other radio installations, buildings and trees, because of sloping and uneven ground and ground with varying electrical properties. Usually the most accurate estimates of G_t and G_r are obtained from experimental measurements or from a combination of measurement and theory. Such values should be used whenever available. However, more commonly direct recourse must be made to fully theoretical values.

Unfortunately also, existing theoretical estimates of antenna gains tend to be subject to certain limitations. Many are based on the assumption that the antenna is situated over perfectly conducting ground, whereas at HF the finite ground conductivity and dielectric constant can have a marked effect on the antenna performance. Usually more accurate figures are obtained with assumed values of these ground constants.

Although most antennae are designed to radiate or receive horizontally or vertically polarized waves along the great-circle path between transmitter and receiver, in other directions the waves in general are elliptically polarized. Since the power coupling to the ordinary and extraordinary waves in the ionosphere depends on the wave polarizations to which the antennae respond, these polarizations should be specifically determined. This is particularly important for example in assessing the interfering effects of a transmitter in a non-great circle direction. A convenient way of expressing antenna performance would be to specify the separate gains for horizontally and vertically-polarized waves, together with the wave relative-phases. Unfortunately, such data are not currently available. Each antenna must then be regarded as radiating or receiving entirely horizontally or vertically polarized signals, whichever provides the closer approximation to the situation under investigation.

Equations for G_t and G_r given by Barghausen *et al.*, [1969], used and extended by Haydon *et al.*, [1976], are incorporated in the present method. Gains are expressed in decibels relative to an isotropic antenna in free space. The equations apply for antennae situated over horizontal uniformly flat ground of finite conductivity and are for the following basic antenna types:

— constant gain antenna;
— horizontal terminated rhombic;
— grounded vertical monopole;
— horizontal half-wave dipole;
— horizontal Yagi with any number of elements;
— vertical dipole;
— curtain array with a perfectly conducting screen consisting of any number of bays, vertical and horizontal spacings;
— terminated sloping V;
— inverted L;
— terminated sloping rhombic;
— sloping long wire;
— horizontal log-periodic;
— dipole of any length, orientation in azimuth and elevation angle;
— vertical half rhombic;
— sloping double rhomboid, and
— grounded vertical monopole with radial conducting mat.

Provision is also included for an antenna pattern specified by a matrix of numbers, and for a vertical loop antenna.

7.2 *Spatial attenuation, L_d*

Spatial attenuation arises from the spreading of power flux over an increasing area during signal propagation; in free space the power flux-density is inversely proportional to the square of the path length. For rays in the ionosphere,

however, refraction modifies this and leads to both focussing and defocussing. Defocussing tends to be associated with refraction below the reflection height and with signals propagated via high-angle (Pedersen) rays. It is not considered appropriate to attempt to include allowances for defocussing which is usually of only limited importance since it usually arises under fringe conditions close to geometrical cut-off. There are three different situations where focussing occurs—for rays of low elevation angle, at frequencies close to the MUF, and near the antipodes. No allowance is made for the second of these because MUF focussing is a transitory feature likely to be effective only for restricted conditions.

It is convenient to regard spatial attenuation L_d, defined with respect to the signal at a distance of 1 km from the transmitter along the ray path direction, as consisting of two components: and equivalent free-space path attenuation L_f and a focus gain G_f, such that

$$L_d = L_f - G_f \tag{34}$$

where all quantities are expressed in decibels.

The equivalent free-space path for a particular mode is taken to have a length equal to the mirror-reflecting slant path between transmitter and receiver. Hence, for an n-hop mode:

$$L_f = 20 \log \left[2R \sum_n \frac{\sin \frac{d_r}{2R}}{\cos \left(\Delta'_r + \frac{d_r}{2R} \right)} \right] \quad \text{dB} \tag{35}$$

where Δ'_r is the mean elevation angle on the upward and downward legs of the rth hop of ground-range span d_r.

R is the radius of the Earth in km.

The mean allowances for horizon focussing of rays of low elevation angle for E and F-modes, deduced by Bradley [1970] for idealized model ionospheres are taken. These give G_f as a function of the mean elevation angle of the upgoing rays over all hops, as shown in Fig. 6. It is independent of the number of wave hops and reaches a maximum (determined by ionospheric roughness) of 9 dB at grazing incidence.

In the case of propagation to very long distances with D, the great-circle distance between transmitter and receiver, greater than $\pi R/2$, focussing is taken into account by means of the following provisional formula [Hortenbach and Rogler, 1979]:

$$G_f = 20 \log \left(\left| 1 - \frac{n\pi R}{D} \right| \right) \quad \text{dB} \tag{36}$$

for $\left(\frac{2n-1}{2} \right) \pi R \leqslant D \leqslant \left(\frac{2n+1}{2} \right) \pi R$ with $n = 1$ and 2.

As G_f given by equation (36) tends to infinity for $D = n\pi R$ it is limited arbitrarily to the value of 30 dB.

7.3 *Ionospheric absorption*

Ionospheric waves are subject to absorption. In the case of vertical-incidence propagation at a frequency f_v (MHz) the absorption of the ordinary wave, $L(f_v)$, is given approximately from magnetoionic theory by the expression for quasi-longitudinal propagation:

$$L(f_v) = 2.33 \times 10^{-15} \int \frac{N\nu}{\mu} \times \frac{\mathrm{d}h}{(f_v + f_l)^2} \quad \text{dB} \tag{37}$$

N: electron concentration in electrons/m^3;
ν: electron-collision frequency in s^{-1};
μ: refractive index;
f_l: electron gyro-frequency in MHz about the component of the Earth's magnetic field along the direction of propagation (taken as positive).

The height limits of the integration are from the base of the ionosphere to the appropriate height of reflection at frequency f_v. This equation shows that the absorption depends on the height distribution of electron concentration and that it can be large near the height of reflection where $\mu \ll 1$. It is convenient to refer to absorption as non-deviative when $\mu \approx 1$ and deviative in other cases.

Normal non-deviative absorption arises as a result of ionisation produced by the regular solar radiation. At temperate latitudes in the winter, the non-deviative absorption becomes anomalously high and subject to greater day-to-day variability than would be expected from a normal solar control. The effect is not yet fully understood and is referred to as winter-anomaly absorption. It has been studied extensively in the Federal Republic of Germany [Dieminger *et al.*, 1966; Schwentek, 1966, 1967, 1968, 1971] and in Japan [Wakai *et al.*, 1970, 1974]. At high latitudes there is additional non-deviative absorption arising from the incidence of electrons and solar protons precipitating from the magnetosphere under disturbed conditions. These lead to enhanced D-region ionisation and give the phenomena of auroral and polar-cap absorption. The types of absorption taken into account in the present prediction method are normal non-deviative and deviative absorption (including median winter-anomaly absorption) and auroral absorption.

7.3.1 *Non-deviative and deviative absorption, L_a*

The estimation of the non-deviative and deviative absorption is based on an analysis of vertical-incidence absorption measurements [George, 1971] and uses the results of ray-tracing calculations through model ionospheres, which lead to a relationship between the absorption at vertical and oblique incidence [George and Bradley, 1973]. The procedure has been described in detail by George and Bradley [1974]. This takes no account of absorption in the F-region arising from collisions between electrons and ions, but Rush and Elkins [1975] have shown that the total F-region absorption due to both electron-ion and electron-neutral atmosphere collisions for a single-hop path is usually less than 1 dB. An exception is the case of the high-angle ray, which is not considered in this prediction procedure.

The absorption L_a experienced by the ordinary wave of frequency f_{ob} reflected from the ionosphere obliquely is given in terms of the absorption $L_a(f_v)$ of the ordinary wave at vertical incidence on a related frequency f_v by

$$L_a = \frac{A\ (f_v) \times \sec\ i_{100}}{(f_{ob} + f_l)^2} \tag{38}$$

where $A(f_v) = L_a(f_v) \times (f_v + f_l)^2$. The term f_l is now the electron gyrofrequency about the vertical component of the Earth's magnetic field, and it is taken as being positive. f_v is given in terms of f_{ob} by

$$f_v = f_{ob} \times \cos\ i_{100} \tag{39}$$

i_{100} is the zenithal angle of the unrefracted oblique ray projected to a height of 100 km, so that

$$i_{100} = \arcsin (0.985 \cos \Delta) \tag{40}$$

where Δ is the angle of elevation of the ray at the ground.

George [1971] has shown that at noon $A(f_v)$ is related to A_T, the limiting value of $A(f_v)$ for a sufficiently high frequency that the signals traverse the whole of the absorbing region without deviation, as a function of the ratio of f_v to foE. With

$$\frac{A\ (f_v)}{A_T} \equiv \varphi_n \left(\frac{f_v}{\text{foE}}\right) \tag{41}$$

the function φ_n is approximately independent of location, season or solar epoch and it is given from George's results as indicated in Fig. 7. In particular, this holds under normal absorption conditions and it also applies approximately for winter-anomaly absorption. Samuel and Bradley [1975] have shown that its use may be extended to other times of day than noon.

Now for a given month and location, A_T increases linearly with twelve-month running mean sunspot number R_{12} and changes diurnally as a function of χ, the solar-zenith angle. $A_T(R_{12}, \chi)$ is related to $A_T(0,0)$ in the daytime by:

$$A_T(R_{12}, \chi) = A_T(0,0) \times F(\chi) \times (1 + 0.0067\ R_{12}) \tag{42}$$

where $F(\chi) = \cos^p(0.881\chi)$. The parameter p is a function of month and of the modified dip latitude $|X|$, as given in Fig. 8. The parameter X is that used in the mapping of foF2 and is defined in equation (5).

Hence, combining equations (38), (41) and (42) gives:

$$L_a = \frac{\varphi_n \left(\frac{f_v}{\text{foE}}\right) \times A_T\ (0,0) \times F\ (\chi) \times (1 + 0.0067\ R_{12}) \times \sec\ i_{100}}{(f_{ob} + f_l)^2} \quad \text{dB} \tag{43}$$

A map produced by George [1971] from observational data gives $A_T(0,0)$ for each month of the year and as a function of $|X|$. This is shown in Fig. 9. Hence, using numerical representations of the curves of Figs. 7 to 9 and equation (43), the daytime oblique-path absorption of the ordinary wave is given. For a multiple-hop mode the absorption on each

hop is evaluated separately taking mid-hop position ionospheric characteristics and a mean elevation angle for the upward and downward legs of the hop. At high latitudes with $|X| > 70°$, values of $A_T(0,0)$ and p are taken as for $X = 70°$.

Mid-latitude winter absorption values derived by this procedure have been compared with figures given by an empirical formula which has been fitted to experimental data recorded at a frequency of 2.6 MHz over a 300 km range path in the Federal Republic of Germany [Rottger and Schwentek, 1974]. Some systematic differences of up to 6 dB are revealed, particularly at sunspot minimum, which require further investigation. However, these tests provide some support for adopting the above procedure for provisional use.

After sunset the absorption falls to a small non-zero value. Night-time absorption has been studied extensively in Japan [Wakai, 1961, 1971; Wakai *et al.*, 1971] using experimental measurements of the field strengths of standard transmitters over a continuous range of distances up to 14 000 km. These data indicate [Wakai, 1975] that the residual night-time absorption of the ordinary wave is given approximately as:

$$L_a = \frac{(7 + 0.019\,D)\;(1 + 0.015\,R_{12})}{f_{ob}^2 + 10} \quad \text{dB} \tag{44}$$

f_{ob} is the wave frequency in MHz and D is the transmission range in km. This equation shows L_a increasing linearly with D and strictly for any transmission range should be interpreted as relating to the resultant signal. However, for application to the present procedure, the values determined are regarded as applying separately to each of the propagation modes that can exist. Equation (44) is taken for those times when it gives a larger absorption than that derived from equation (43).

7.3.2 *Auroral absorption, L_h*

Sky-wave signals which traverse the auroral zones can be subject to large amounts of absorption. Auroral absorption is associated with increases in electron concentration produced by energetic electrons incident during substorms. Although the greatest absorption results from the most intense substorms, it is believed that in the auroral regions it is physically realistic to assume the existence of an ensemble of absorption enhancements associated with a corresponding ensemble of substorms. The numbers and intensities of substorms are assumed to be such that although the day-to-day absorption variability is greater than at other latitudes, the monthly median absorption shows statistically stable temporal and spatial features that can meaningfully be represented numerically. Equations are given below to estimate this absorption.

The method of prediction of auroral absorption given by Foppiano [1975] is adopted. This method makes use of riometer data which form the majority of all auroral absorption measurements. Riometers are instruments with upward directed antennae, usually operating at frequencies around 30 MHz, which detect changes in the incident cosmic-noise flux [Little and Leinbach, 1959]. Riometer data are related to the equivalent values of absorption on oblique-propagation paths using the results of ray-tracing calculations for representative model ionospheres.

Equations have been fitted to published riometer data from 27 stations in the Northern hemisphere to indicate the spatial and temporal variations of the auroral absorption. Mapping is in terms of a coordinate system of corrected geomagnetic latitude φ, corrected geomagnetic longitude θ and corrected geomagnetic local time T [Hakura, 1965]. Although auroral absorption may have a somewhat different morphology in the Southern hemisphere because of differences in the Earth's magnetic field, as an interim measure the equations are to be used in both hemispheres.

Q_1, which is the percentage probability that the absorption measured at 30 MHz exceeds 1 dB for a riometer with an antenna pointing at the zenith, is given as the sum of two separate terms, Q_{1d} and Q_{1s}. These terms correspond respectively to absorption contributions which are assumed to arise from two different sorts of incident auroral particles, referred to as "drizzle" and "splash" [Hartz and Brice, 1967]. Since the sources, energies and incident directions of these particles differ, the two terms have different spatial and temporal statistics.

Empirical equations based in part on the known particle statistics and on riometer data give

$$Q_1 = Q_{1d} + Q_{1s} \tag{45}$$

with

$$Q_{1d} = 21\; d_\varphi \cdot d_T \cdot d_R \cdot d_\theta \cdot d_M \tag{46}$$

and

$$Q_{1s} = 12\; s_\varphi \cdot s_T \cdot s_R \cdot s_\theta \cdot s_M \tag{47}$$

The suffixes φ, T, R, θ and M relate to terms which have a principal dependence on latitude, time of day, solar activity, longitude and season, respectively. The terms are given as follows:

(*a*) $$d_\varphi = \exp\left[\frac{-(\varphi - \varphi_m)^2}{2\sigma_\varphi^2}\right] \quad \text{with } \varphi \text{ in degrees} \tag{48}$$

where $$\varphi_m = 68\ (1 - 0.0004\ R_{12}) \quad \text{degrees} \tag{49}$$

and $$\sigma_\varphi = 3\ (1 + 0.004\ R_{12}) \quad \text{degrees} \tag{50}$$

R_{12} is the twelve-month running mean sunspot number.

$$\mathrm{d}_T = \exp\left[\frac{-(t_1 - T_m)^2}{15.7}\right] \tag{51}$$

where $$T_m = 10\ (1 - 0.002\ R_{12}) \quad \text{hours} \tag{52}$$

T is in hours in the range 0 to 24 such that:

$$t_1 = T \quad \text{for } 0 \leqslant \mathrm{T} \leqslant (12 + T_m)$$
$$t_1 = T - 24 \quad \text{for } (12 + T_m) < T < 24 \tag{53}$$

$$d_R = 1 + 0.014\ R_{12} \tag{54}$$

$$d_\theta = \begin{cases} 0.58 - 0.42 \sin\left[0.947\ (\theta + 85°)\right] & \text{for } 0 \leqslant \theta < 10 \\ 0.16 & \text{for } 10 \leqslant \theta < 80 \\ 0.58 + 0.42 \sin\left[1.80\ (\theta - 130°)\right] & \text{for } 80 \leqslant \theta < 180 \\ 0.58 - 0.42 \sin\left[0.947\ (\theta - 275°)\right] & \text{for } 180 \leqslant \theta < 360 \end{cases} \tag{55}$$

where θ is in degrees E of Greenwich in the range 0 to 360.

$$d_m = 1 - 0.3 \sin 3.86\ \delta \tag{56}$$

where δ is the mean solar declination for the month in degrees

(*b*) $$s_\varphi = \exp\left[-\frac{(\varphi - \varphi'_m)^2}{2\sigma_\varphi^2}\right] \tag{57}$$

where $\varphi'_m = 67\ (1 - 0.0006\ R_{12}) + 0.3\ (1 + 0.012\ R_{12})|t|$ degrees (58)

$$t = T - 3 \quad \text{for } 0 \leqslant T \leqslant 15$$
$$t = T - 27 \quad \text{for } 15 < T < 24 \tag{59}$$

$$s_T = \exp\left[-\frac{t_2^2}{15.7}\right] \tag{60}$$

where $$t_2 = T \quad \text{for } 0 \leqslant T \leqslant 12$$
$$t_2 = T - 24 \quad \text{for } 12 < T < 24 \tag{61}$$

$$s_R = 1 + 0.009\ R_{12} \tag{62}$$

$$s_\theta = d_\theta \tag{63}$$

$$s_m = 1 \tag{64}$$

Riometer data are found to follow approximately a fixed relationship between Q_1 and A_m, the median absorption. With Q_1 as a percentage and A_m in decibels:

$$A_m = \left(\frac{Q_1 + 30}{80}\right)^{1.54} \quad \text{for } Q_1 \geqslant 1$$
$$A_m = 0.23\ Q_1^{0.2} \quad \text{for } Q_1 < 1 \tag{65}$$

Measurements are influenced in a complicated way by calibration procedures, the effect of the finite size of the ionisation enhancements which cause auroral absorption and the angular range of incident cosmic noise within the antenna beamwidth. However, theoretical computations suggest that to a first approximation the absorption measured with a riometer is equal to that experienced at the same frequency by a vertically propagated signal making a single traverse of the lower ionosphere.

If L_{30} is the vertical-incidence absorption for a single ionospheric traverse at a frequency of 30 MHz, the corresponding absorption L_f at some other frequency f is taken as

$$L_f = L_{30} \left(\frac{30 + f_l}{f + f_l}\right)^2 \times \varphi_n \left(\frac{f}{\text{foE}}\right) \tag{66}$$

where f_l is the electron gyrofrequency about the vertical component of the Earth's magnetic field. The function $\varphi_n\left(\frac{f}{\text{foE}}\right)$ is given in § 7.3.1.

The auroral absorption for a single-hop oblique sky-wave mode is expressed in terms of the sum of the values of absorption at vertical incidence for the upgoing and downcoming legs of the path; these values are derived separately as a function of the Q_1 and foE appropriate to the geographic positions where the ray path attains a height of 100 km. The oblique-path absorption $L(f_{ob})$ at frequency f_{ob} is given in terms of this summed vertical-incidence absorption $L(f_v)$ for frequency f_v by:

$$L(f_{ob}) = L(f_v) \times \left(\frac{f_v + f_l}{f_{ob} + f_l}\right)^2 \times \sec\ i_{100} \tag{67}$$

f_l is the electron gyrofrequency about the vertical component of the Earth's magnetic field and i_{100} is the zenith angle of the oblique ray path at a height of 100 km. f_v is chosen so that

$$f_v = f_{ob} \times \cos\ i_{100} \tag{68}$$

In the auroral zone the absorption determined by this procedure represents the total absorption and in general for an n-hop mode it is the sum of that for the separate hops:

$$L_h + L_a = \sum_n L(f_{ob}) \tag{69}$$

with $L(f_{ob})$ given for each hop from equation (67) above. To allow in the summation for multiple-hop paths where some hops are outside the auroral zone, a separate comparison is made for each hop between the estimated values of auroral absorption and of non-deviative and deviative absorption derived in accordance with § 7.3.1; the greater value is taken as applying.

7.4 *Polarization-coupling loss and multiple-hop ground-reflection loss, L_c*

In general, when an upgoing wave is incident on the ionosphere it leads to the excitation of an ordinary (O) and an extraordinary (X) wave. These two waves have different polarizations, may be regarded as propagating independently within the ionosphere, and are subject to different amounts of absorption. Although ground-reflection losses depend on wave polarization, here values are taken for circularly polarized waves. Polarization-coupling losses, multiple-hop ground losses and absorption losses are examined together.

7.4.1 *Single-hop modes*

First consider single-hop propagation over a path as shown in Fig. 10 between a transmitter at T and receiver at R. A and B are the positions of wave entry to and exit from the ionosphere respectively. The wave launched at T travels through the free space to A with unchanged polarization. At A an O and an X wave are excited and these are propagated independently along similar ray paths to B. At all positions along the ray paths in the ionosphere, the O and X wave polarizations change so as to remain characteristic waves, but between B and R these polarizations are unchanged and equal to the so-called limiting polarizations at B. The fractions of power coupled to the O and X waves and the fractions of power in the downcoming waves coupled to the receiving antenna at R depend on the limiting polarizations of the O and X waves at A and B and on the polarizations to which the transmitting and receiving antennae respond. The downcoming waves propagated as O and X waves within the ionosphere are assumed to have random relative phases so that their received powers are additive.

When the transmitting and receiving antennae radiate linearly polarized waves and propagation is quasi-longitudinal to the Earth's magnetic field, so that the limiting polarizations are circular, the effective polarization-coupling loss ranges from 3 to 6 dB, depending on the differential absorption of the X wave relative to the O wave. Under other conditions when the limiting polarizations are elliptical, when there is poor coupling between the transmitting antenna and the O wave, and when the X wave is heavily attenuated, polarization-coupling losses are large. Curves of single-hop polarization-coupling losses for different propagation directions in different geographical regions have been presented by Bradley [1968]. These show that losses can exceed 20 dB under some conditions and confirm that it is important to include a full calculation in the prediction procedure.

A method of calculation has been described by Moorat [1968] where the transmitting and receiving antennae radiate and respond to waves which are either horizontally or vertically polarized. Let a be the fraction of power coupled to the O wave from an antenna which radiates horizontally polarized waves and let b be the fraction of the power at R from the downcoming O wave coupled to a receiving antenna which responds to horizontally polarized waves. Let α_O and α_X be the fractional power absorptions of the O and X waves respectively over the path. Then for different combinations of horizontal and vertical wave polarizations to which the transmitting and receiving antennae respond, the fractions of power coupled to the receiving antenna are as indicated in Table II.

TABLE II – *Fractions of power coupled to receiving antenna for single-hop mode*

Exciting wave polarization	Received wave polarization	Fractional power at receiver
Horizontal	Horizontal	$ab\alpha_O + (1-a)(1-b)\alpha_X$
	Vertical	$a(1-b)\alpha_O + (1-a)b\alpha_X$
Vertical	Horizontal	$(1-a)b\alpha_O + a(1-b)\alpha_X$
	Vertical	$(1-a)(1-b)\alpha_O + ab\alpha_X$

a is given in terms of the O wave limiting polarization ρ_{ol} and angle ε_l between the major axis of the O wave ellipse and the horizontal direction in the plane of the wavefront at A as:

$$a = \frac{\cos^2 \varepsilon_l + |\rho_{ol}|^2 \sin^2 \varepsilon_l}{1 + |\rho_{ol}|^2} \tag{70}$$

b is similarly given by the corresponding expression for a wave polarization ρ_{or} and polarization ellipse major axis inclination ε_r appropriate to position B. ρ_{ol} and ρ_{or} are determined by applying at A and B respectively the general expression for limiting polarization ignoring electron collisions:

$$\rho_o = j\,(\pm\sqrt{1 + Z_C^2} - Z_C) \tag{71}$$

The positive sign is taken when the Earth's magnetic field has a component along the direction of propagation and the negative sign when in the reversed sense.

$$Z_C = \frac{Y_T^2}{2\,Y_L} \text{ with } Y_T = Y \sin \Theta, \quad Y_L = Y \cos \Theta \text{ and } Y = \frac{f_H}{f}$$

f: wave frequency;
f_H: total gyrofrequency;
Θ: angle between the direction of propagation and the Earth's magnetic field.

In the absence of electron collisions the major axis of the O waves ellipse is parallel to the projection of the Earth's magnetic field onto the wavefront plane. Θ and ε are given in terms of the field and ray path directions by standard expressions [Moorat, 1968].

For an ordinary-wave absorption $L_{aO} = -10 \log \alpha_O$ given by the equations of § 7.3, the corresponding extraordinary-wave absorption $L_{aX} = -10 \log \alpha_X$ is assumed related to L_{aO} by:

$$\frac{L_{aO}}{L_{aX}} = \frac{(f + f_{lu})^{-2} + (f + f_{ld})^{-2}}{(f - f_{lu})^{-2} + (f - f_{ld})^{-2}} \tag{72}$$

f_{lu} and f_{ld} are the electron gyrofrequencies (taken as positive) about the components of the Earth's magnetic field along the direction of propagation at A and B on the upwards and downwards legs of the path respectively.

7.4.2 *Multiple-hop modes*

In the case of multiple-hop modes all the considerations given in § 7.4.1 for single-hop modes apply, but additional allowances should be made for the loss of power at ground reflection and for the effective transfer of power between the O and X waves on successive hops arising from the mode conversion which takes place at each entry to the ionosphere. However, these calculations become rather lengthy [Bradley and Bramley, 1971] and so in the present method only

allowances for ground-reflection losses of circularly-polarized waves are included, together with the polarization-coupling losses calculated as for single-hop modes.

For a circularly-polarized downcoming wave the ground-reflection loss is

$$10 \log \left(\frac{|R_H|^2 + |R_V|^2}{2} \right) \qquad \text{dB}$$

where R_H and R_V are the Fresnel-reflection coefficients for horizontal and vertical-wave polarizations, respectively. These are given by

$$R_H = \frac{\sin \Delta - (n^2 - \cos^2 \Delta)^{\frac{1}{2}}}{\sin \Delta + (n^2 - \cos^2 \Delta)^{\frac{1}{2}}} \tag{73a}$$

and

$$R_V = \frac{n^2 \sin \Delta - (n^2 - \cos^2 \Delta)^{\frac{1}{2}}}{n^2 \sin \Delta + (n^2 - \cos^2 \Delta)^{\frac{1}{2}}} \tag{73b}$$

where Δ is the elevation angle of the downcoming wave. n is the complex refractive index given in terms of wave frequency f (MHz), ground conductivity σ (S/m) and relative dielectric constant ε_r by

$$n^2 = \varepsilon_r - \mathrm{j} \frac{18000}{f} \sigma \tag{74}$$

σ and ε_r are specified from a numerical map of land-sea boundaries based on formulae originally developed to describe the geographic variations of atmospheric noise intensity [Zacharisen and Jones, 1970]. This map gives $\sigma = 5$ S/m, $\varepsilon_r = 80$ over the sea, $\sigma = 0.01$ S/m, $\varepsilon_r = 10$ well inland and $\sigma = 0.0001$ S/m, $\varepsilon_r = 1$ for ice. There is a gradual transition between these limiting values near the land-sea and ice-sea boundaries, which is consistent with the use of a median ionospheric model in the predictions, whereas in practice day-to-day changes sometimes make the reflection point lie on land and sometimes on the sea or ice. Values of σ and ε_r are generated appropriate to each ground-reflection point indicated by the ray path determination procedure of § 6.3 and hence the corresponding ground-reflection losses are determined.

7.5 *Sporadic-E obscuration and reflection losses*

The determination of sporadic-E obscuration and reflection losses is made difficult because there are limitations in both theoretical and practical approaches. Theoretical assessments are restricted by the applicability of assumed models of the structure of Es irregularities; experimental data require several assumptions for their interpretation because sporadic-E losses cannot be directly measured independently of other transmission losses. In addition, since the term sporadic-E refers to a number of different types of ionospheric irregularities with separate physical causes, these are likely to have different characteristics and therefore to yield different orders of losses.

Although it seems probable that the vertical-incidence ionospheric characteristic foEs is the best single parameter descriptive of the reflecting properties of an Es layer and that fbEs more appropriately describes the obscuration properties, this is not definitely established. In the long term, experimental studies such as those recently commenced in Finland [Turunen, 1975], where reflection losses at vertical incidence are being measured in conjunction with simultaneously recorded ionograms indicating the types of Es irregularity present, appear to offer great potential for improved prediction procedures. For the present, however, allowances must be used based on somewhat limited amounts of data.

7.5.1 *Obscuration loss, L_q*

Whereas it is to be noted (see §§ 6.1 and 6.4) that no allowance is made for the possible blanketing and refraction by the sporadic-E layer of F-mode signals, obscuration losses are taken into account using an empirical equation developed by Sinno *et al.*, [1976]. An analysis of vertical and oblique-path HF signal-strength data recorded at night when regular mode propagation was not possible and absorption losses were small, has led to the expression for L_q, the obscuration loss for a single traverse of the Es layer, as:

$$L_q = -10 \log (1 - R^2) \qquad \text{dB} \tag{75}$$

where

$$R = \frac{1}{1 + 10\left(\dfrac{f}{\text{foEs} \times \sec i_{110}}\right)^8} \qquad (76)$$

f is the wave frequency in MHz and i_{110} is the zenith angle of the oblique ray at a height of 110 km. In particular this equation gives $L_q = 0.04$ dB for $f = \text{foEs} \times \sec i_{110}$ and $L_q \to \infty$ as $f \to 0$. The total obscuration loss is determined by summing the values of L_q evaluated separately for each leg of each hop. Monthly median obscuration loss is given substituting monthly median values of foEs in equation (76). This loss is to be computed for all F-modes at or below the greatest MUF and for any distance.

7.5.2 *Reflection loss, L_r*

Measured signal-strength data collected mainly at VHF for a whole range of middle-latitude paths have been analyzed. A procedure for estimating sporadic-E reflection losses has been developed by Miya and Sasaki [1966]. This procedure has been revised and extended by Interim Working Party 6/8 (Recommendation 534; [Miya *et al.*, 1978]). Mean relationships for sporadic-E reflection losses are shown in Fig. 11 assuming that antenna beamwidths are sufficiently wide that there is no appreciable restriction of the area of sporadic-E cloud illuminated. L_r as shown is expressed in terms of the midpath value of foEs and corresponds to single-hop propagation for transmission ranges up to 2600 km and to two-hop propagation for greater ranges up to 4000 km. Use of monthly median values of foEs gives estimates of the monthly median reflection loss. It has been noted in § 6.1 that signal contributions from sporadic-E modes are taken into account only for these transmission ranges and for frequencies above the path MUF.

Since such frequencies are relatively large, it is assumed that absorption losses are small and that no separate allowance for these should be included in the transmission-loss determination. The curves of Fig. 11 are interpreted as already incorporating mean allowances for ionospheric absorption, focussing and polarization-coupling loss. Hence, in particular, losses for a two-hop mode are not double those indicated for a single hop over half the path length. Fig. 11 is provisionally taken as applying for all latitudes.

7.6 *Loss associated with propagation at frequencies above the MUF, L_m*

Strong signals are often received at frequencies above the standard MUF. Ignoring prediction errors, there are a number of different reasons why this should be so. Firstly, it must be recognized that predicted values are monthly median figures, so that for half the days the ionosphere can support higher frequencies. Then, it has been shown [Miya *et al.*, 1951; Miya and Kanaya, 1955] that at frequencies above the standard MUF, significant signal contributions arise via paths which involve sidescatter from ground irregularities. Such paths are often significantly longer than the corresponding great-circle paths and some have appreciably greater MUF. Additionally, signals which involve reflection from the sporadic-E layer may be received at frequencies above the standard MUF. Even for reflection from the regular F-layer it has been suggested [Wheeler, 1966] that it is legitimate to regard this layer as composed of a number of separate patches of ionisation with differing maximum electron concentrations, so that each patch has its own MUF. Hence the number of patches supporting wave reflection falls with increase of frequency and there is no single frequency giving an abrupt signal cut-off.

The present prediction method makes a separate allowance for sporadic-E mode signals (see § 7.5.2) and field strengths are taken as those applying for sporadic-E modes when their estimated intensities exceed those attributed to signals which propagate by other mechanisms. At present, no specific allowance is incorporated for sidescatter modes and the combined effect of the other mechanisms is incorporated using empirical equations derived from observational field-strength data.

There is experimental evidence [Dieminger and Rose, 1961] that the rate of decrease of field strength above the standard MUF depends on path length and on whether the ionosphere is disturbed. Although often the frequency beyond which field strengths decrease lies somewhat below the standard MUF, this feature is not yet taken into account. An additional loss term L_m is introduced only for frequencies above the standard MUF.

Analysis of signal measurements in the United States of America indicates that transmission loss increased parabolically with increase of frequency for frequencies above the standard MUF, in agreement with the Phillips-Abel theory [Wheeler, 1966]. For wave frequencies $f >$ MUF data are consistent with

$$L_m = 130\left(\frac{f}{\text{MUF}} - 1\right)^2 \quad \text{dB} \qquad (77)$$

Work is in progress in the Federal Republic of Germany [Damboldt, 1976] and in Japan [Kanaya and Wakai, 1976] which may lead to a more accurate method of estimating L_m.

7.7 *Additional losses, L_z*

Each of the loss terms discussed in the previous sections is important under some conditions. Provision is made by the inclusion of an additional loss term L_z, initially set to 0 dB, to allow empirically for any extra losses, such as for example due to scattering from spread-F irregularities, which may emerge as significant. The inclusion of L_z provides a simple means of correcting the prediction system in the light of experience gained from its use. Also, the determination of values of L_z from limited sets of experimental data is a convenient way of comparing results in advance of a full analysis to identify any sources of discrepancies and to determine explicit ways of correcting for these.

8. Overall transmission loss and field strength of downcoming sky-waves at receiving site

In this section the losses arising from the separate effects discussed in § 7 are combined and, using standard relationships, equations are developed leading to the determination of the overall transmission loss and the field strength of the downcoming sky-waves at the receiving site.

8.1 *Basic free-space transmission loss, L_{bf}*

Basic free-space transmission loss is defined as the radio of the ratio frequency power radiated from an ideal loss-free isotropic transmitting antenna to the resultant radio frequency signal power which would be available from an ideal loss-free isotropic receiving antenna for a path length in free space equal to that of the practical system under consideration. Annex I to Recommendation 525 gives:

$$L_{bf} = 20 \log \left(\frac{4\pi d}{\lambda}\right) \quad \text{dB} \tag{78}$$

for a path length d, where λ is the wavelength in the same units.

The corresponding expression for a wave of frequency f in MHz is

$$L_{bf} = 32.4 + 20 \log f + 20 \log d \quad \text{dB} \tag{79}$$

where d is expressed in km. In particular, for an ionospheric mode it is given from equation (35) as

$$L_{bf} = 32.4 + 20 \log f + L_f \quad \text{dB} \tag{80}$$

where L_f is the free-space path attenuation with respect to a distance of 1 km from the transmitter in dB.

8.2 *Basic transmission loss, L_b*

The basic transmission loss, sometimes called the path loss, is defined in Recommendation 341 as the ratio of the radio frequency power radiated to that received, between ideal, loss free, isotropic transmitting and receiving antennae at the same locations as the actual transmitting and receiving antennae. Hence, for a given ionospheric mode

$$L_b = L_{bf} + L_a + L_c + L_h + L_m + L_q + L_r + L_z - G_f \tag{81}$$

This equation shows all the loss factors that may need to be included under different conditions, although not all apply simultaneously for any one mode (see Fig. 2).

8.3 *Transmission loss, L*

Recommendation 341 defines transmission loss as the ratio of the radio frequency power radiated from the transmitting antenna to that which would be available from the receiving antenna if there were no circuit losses other than those associated with its radiation resistance. So

$$L = L_b - G_t - G_r \tag{82}$$

8.4 *System loss, L_s*

The system loss is defined (Recommendation 341) as the ratio of the radio frequency power input to the terminals of the transmitting antenna to the radio-frequency signal power available at the terminals of the receiving antenna. This excludes any transmitting or receiving antenna transmission line losses, since it is considered that such losses are readily measurable. On the other hand, the system loss includes all of the losses in the transmitting and receiving antenna circuits, including not only the transmission loss due to radiation from the transmitting antenna and re-radiation from the receiving antenna, but also any ground losses, dielectric losses, antenna loading coil losses, terminating resistor losses in rhombic antennae etc.

Let L_{tc} and L_{rc} be the losses, expressed in decibels, in the transmitting and receiving antennae circuits respectively, excluding the losses associated with the antenna radiation resistances, i.e. the definitions of L_{tc} and L_{rc} are $10 \log (r'/r)$, where r' is the resistive component of the antenna input impedance and r is the radiation resistance. So

$$L_s = L + L_{tc} + L_{rc} \tag{83}$$

Theoretical expressions are available for r for some antennae [Barghausen *et al.*, 1969] although it is to be noted that these are relatively complex, and in some cases require the use of numerical integration procedures. Whilst it is often feasible to make a nominal allowance for some of the factors which determine r' from a knowledge of the antenna structure and feed arrangements, r' can usually only be evaluated precisely from direct *in-situ* measurements. Hence, it is not possible to extend the prediction procedure to the estimation of system loss. For accurate comparisons with predictions, measured signal-strength data should be supplemented with measurements of r'.

8.5 *r.m.s. sky-wave field strength*

Let the radio-frequency power input to the terminals of the transmitting antenna be P_t and the radio-frequency signal power available at the terminals of the receiving antenna be P_a, with both quantities expressed in decibels relative to 1 watt. Then

$$P_a = P_t - L_s \qquad \text{dBW} \tag{84}$$

or, if antenna losses other than those associated with radiation resistances are ignored,

$$P_a \approx P_t - L \qquad \text{dBW} \tag{85}$$

If F is the r.m.s. field strength of a downcoming fading sky-wave expressed in decibels relative to 1 μV/m and P_a is the corresponding mean power, then ignoring receiving antenna losses

$$P_a \approx F + G_r - 120 + 10 \log \left(\frac{1}{30} \times \frac{\lambda^2}{16\pi^2} \right) \tag{86}$$

and

$$F \approx P_t - L - G_r + 20 \log f + 107.2 \qquad \text{dB (μV/m)} \tag{87}$$

where λ is now the wavelength in metres and f is the frequency in MHz.

8.6 *Fading allowance for conversion from r.m.s. to mean or median sky-wave field strength*

Ionospheric signals are subject to fading (see Report 266-4) and for some applications there is a need to estimate the mean or median field strength over a period of an hour.

This may be determined from the r.m.s. value if the form of the amplitude distribution is known. Over short periods (3 to 7 minutes), distribution functions close to the Rayleigh distribution predominate. On the other hand, over periods of 30 to 60 minutes the distribution follows the log-normal law with a decile range close to that for the Rayleigh distribution. For the Rayleigh distribution the median and mean values are 1.6 dB and 1.1 dB respectively below the r.m.s. value.

8.7 *Summation of powers in active modes and multipath probability*

The component signals which are propagated via different modes have incoherent phases, and hence the resultant signal at the receiver is determined by summing the power in the separate active modes. The modes considered are those with an availability equal to or greater than 5%.

Each mode should be examined with respect to a minimum tolerable difference in received power, as well as to a maximum tolerable delay time difference, relative to the most reliable mode of transmission, in order to calculate the multipath probability.

8.8 *Day-to-day variations in transmission loss and field strength*

It is recalled that the allowances given in the preceding sections for the ray path transmission loss and gain factors are monthly median values. Day-to-day variations in the overall transmission loss arise from changes in electron concentration: changes in the E- and F-regions influence the ray path directions, thereby affecting the antenna gain, focussing, spatial attenuation, sporadic-E losses and polarization-coupling losses, changes in the D- and E-regions affect the values of ionospheric absorption.

The day-to-day variations of signal strength have been examined for a wide range of paths and operating conditions [Barghausen *et al.*, 1969]. Tables III and IV adapted from their results list the parameters T_u and T_l separately for transmission ranges of less than 2500 km and for greater distances, as a function of midpath local mean time, midpath geomagnetic latitude and season. T_u is the transmission loss exceeded for 10% of the time and T_l is the transmission loss exceeded for 90% of the time, both terms being expressed as deviations from the median transmission loss, L, in decibels.

Assuming that the day-to-day variations follow a χ^2-distribution, the percentage probability P of there being an hourly mean available power at the receiver input greater than some specified value P_{a0}, is given approximately in terms of the monthly median of the hourly mean available powers P_{am} as:

– for $P_{a0} \leqslant P_{am}$

$$P = 130 - \frac{80}{1 + \left(\frac{P_{am} - P_{a0}}{T_u}\right)} \tag{88}$$

or 100, whichever is the smaller.

– for $P_{a0} > P_{am}$

$$P = \frac{80}{1 + \left(\frac{P_{a0} - P_{am}}{T_l}\right)} - 30 \tag{89}$$

or 0, whichever is the larger.

Large deviations in field strength from the median value are to be expected at frequencies above the MUF. The spread in these cases has yet to be determined. As an interim measure the spread is taken the same as at lower frequencies.

TABLE III – *Transmission-loss variability parameters T_u and T_l for transmission ranges less than or equal to 2500 km as a function of season, midpath local time t and midpath geomagnetic latitude G_n (N or S of equator)*

G_n \ t	01-04		04-07		07-10		10-13		13-16		16-19		19-22		22-01		
	T_u	T_l	T_u	T_l	T_u	T_l	T_u	T_l	T_u	T_l	T_u	T_l	T_u	T_l	T_u	T_l	
>75°	12.0	7.2	11.3	9.9	13.1	10.8	13.7	8.1	8.6	6.0	11.0	6.9	14.7	6.3	10.9	6.9	
70-75°	12.0	8.1	19.5	11.4	18.3	12.7	17.8	6.9	9.6	6.1	13.4	8.3	18.9	7.4	11.5	7.7	
65-70°	18.3	9.9	16.9	17.3	28.8	15.1	28.2	7.7	10.5	6.9	14.5	10.0	23.8	10.0	14.7	8.7	
60-65°	17.3	10.2	16.6	16.3	30.3	15.7	26.2	8.7	11.1	7.4	18.0	10.6	22.0	11.4	12.7	9.2	
55-60°	12.8	6.8	12.3	8.6	18.7	10.5	13.6	6.4	9.2	6.1	11.5	8.3	13.6	6.9	12.2	6.5	Winter
50-55°	11.8	6.5	12.4	6.4	13.7	7.6	11.1	7.3	8.8	5.9	11.6	7.4	11.1	7.4	11.9	6.1	
45-50°	11.6	6.0	11.5	5.9	12.3	6.7	10.0	6.5	8.3	5.6	11.0	6.7	10.6	6.7	11.8	5.8	
40-45°	11.5	5.5	10.6	5.5	11.0	5.9	9.1	5.8	7.9	5.4	10.4	5.9	10.1	5.9	11.6	5.4	
<40°	11.5	5.1	9.7	5.1	9.7	5.1	8.2	5.1	8.2	5.1	9.7	5.1	9.7	5.1	11.5	5.1	
>75°	19.8	7.8	23.6	9.6	18.4	12.4	17.4	9.6	15.4	6.9	18.0	7.9	26.4	8.2	20.1	8.1	
70-75°	27.8	9.0	26.6	17.7	25.9	16.4	24.2	11.3	18.2	7.9	23.0	9.2	28.2	11.0	21.1	10.2	
65-70°	35.8	10.4	39.7	14.2	34.4	23.3	35.7	12.8	23.0	9.0	30.7	10.8	36.9	14.5	22.4	14.3	
60-65°	38.8	9.9	37.5	12.2	30.0	17.9	42.2	13.6	24.6	10.6	34.6	13.2	37.1	14.5	34.2	16.6	
55-60°	22.5	7.3	28.2	8.2	19.6	10.6	23.4	9.7	19.8	7.2	25.9	9.6	25.0	9.9	17.0	9.5	Equinox
50-55°	15.6	7.2	21.2	6.7	18.3	10.2	18.2	7.9	17.8	7.2	23.9	9.0	19.2	8.2	15.4	7.9	
45-50°	14.2	6.4	18.0	6.1	15.4	8.4	14.8	6.9	14.6	6.4	19.2	7.7	16.0	7.2	14.1	6.9	
40-45°	12.8	5.8	14.7	5.6	12.5	6.8	11.5	6.0	11.4	5.8	14.5	6.4	12.8	6.1	12.8	6.0	
<40°	11.5	5.1	11.5	5.1	9.7	5.1	8.2	5.1	8.2	5.1	9.7	5.1	9.7	5.1	11.5	5.1	
>75°	16.4	7.3	14.5	7.7	21.5	6.8	12.2	7.3	15.5	6.8	13.1	9.0	15.1	9.2	16.3	8.7	
70-75°	20.0	6.9	19.2	7.4	23.3	8.7	15.4	7.9	17.0	7.0	14.2	8.8	22.8	9.7	20.5	8.7	
65-70°	28.3	8.3	27.9	7.9	34.2	11.8	25.0	8.6	21.2	7.3	17.7	9.2	28.0	10.1	24.3	10.0	
60-65°	31.4	9.6	29.1	7.4	33.3	13.7	24.1	10.0	25.5	7.9	18.2	11.6	26.2	12.9	27.0	11.4	
55-60°	22.8	7.0	20.6	7.0	20.0	9.2	13.6	7.7	17.3	7.4	14.1	10.9	18.0	10.0	19.2	8.2	Summer
50-55°	14.6	6.8	18.7	6.5	15.7	8.1	11.5	7.0	14.8	7.0	13.8	9.3	17.2	8.8	15.4	7.8	
45-50°	13.6	6.1	15.6	6.0	13.7	7.0	10.4	6.4	12.5	6.4	12.4	7.9	14.6	7.6	14.1	6.9	
40-45°	12.5	5.6	12.7	5.5	11.6	6.0	9.2	5.8	10.4	5.8	11.0	6.5	12.2	6.3	12.8	6.0	
<40°	11.5	5.1	9.7	5.1	9.7	5.1	8.2	5.1	8.2	5.1	9.7	5.1	9.7	5.1	11.5	5.1	

Winter: Nov, Dec, Jan, Feb in the N. hemisphere and May, Jun, Jul, Aug in the S. hemisphere.
Summer: May, Jun, Jul, Aug in the N. hemisphere and Nov, Dec, Jan, Feb in the S. hemisphere.
Equinox: Mar, Apr, Sep, Oct in both hemispheres.

TABLE IV – *Transmission-loss variability parameters T_u and T_l for transmission ranges greater than 2500 km as a function of season, midpath local time t and midpath geomagnetic latitude G_n (N or S of equator)*

G_n \ t	01-04		04-07		07-10		10-13		13-16		16-19		19-22		22-01		
	T_u	T_l	T_u	T_l	T_u	T_l	T_u	T_l	T_u	T_l	T_u	T_l	T_u	T_l	T_u	T_l	
>75°	11.8	6.5	10.4	7.6	13.1	7.3	11.8	6.1	9.0	5.6	9.6	6.4	10.5	6.1	12.4	6.4	
70-75°	12.4	4.4	10.0	8.3	14.3	8.7	14.3	6.1	9.1	6.0	9.5	6.9	11.0	6.5	11.8	8.3	
65-70°	13.1	8.3	14.0	8.1	18.2	10.6	20.2	5.6	9.9	6.5	9.3	7.9	10.9	7.8	14.2	11.0	
60-65°	14.6	7.3	12.2	8.7	18.0	9.3	19.5	6.7	10.6	5.2	10.2	8.6	11.4	7.2	17.7	10.0	
55-60°	12.3	6.0	10.6	7.0	15.9	7.2	13.3	6.7	9.5	5.9	9.7	7.0	10.1	6.4	12.5	6.8	Winter
50-55°	12.2	5.9	10.5	6.4	15.2	6.1	11.8	5.9	8.8	5.2	10.1	6.5	9.7	6.3	9.7	6.3	
45-50°	11.9	5.6	10.2	5.9	13.3	5.8	10.5	5.6	8.6	5.2	10.0	6.0	9.7	5.9	12.0	5.9	
40-45°	11.6	5.4	10.0	5.5	11.5	5.4	9.3	5.4	8.3	5.1	9.9	5.5	9.7	5.5	11.8	5.5	
≤40°	11.5	5.1	9.7	5.1	9.7	5.1	8.2	5.1	8.2	5.1	9.7	5.1	9.7	5.1	11.5	5.1	
>75°	14.1	6.1	11.5	5.9	13.6	7.3	13.1	8.1	14.3	7.3	14.1	7.8	17.5	6.9	19.7	8.8	
70-75°	16.8	6.3	12.5	6.8	14.0	7.8	13.4	9.1	15.0	8.6	15.6	8.8	17.7	7.7	20.2	10.0	
65-70°	18.3	7.3	13.6	8.4	17.7	9.9	15.9	10.4	20.6	9.6	16.9	11.0	18.3	10.9	20.7	10.8	
60-65°	19.8	7.3	13.8	7.6	14.6	10.1	17.2	10.9	18.8	11.0	19.5	12.2	18.8	12.5	21.2	12.4	
55-60°	16.9	5.8	13.6	5.9	12.5	7.3	14.3	7.7	16.9	7.2	16.0	10.0	14.8	9.2	17.7	9.6	Equinox
50-55°	15.5	5.6	13.2	5.5	12.4	6.1	14.1	6.9	15.7	6.4	15.2	7.8	14.0	7.0	15.6	7.2	
45-50°	14.1	5.4	12.0	5.4	11.5	5.8	12.0	6.3	13.7	5.9	13.3	6.3	13.1	5.9	14.7	5.6	
40-45°	12.8	5.2	10.9	5.2	10.6	5.4	10.1	5.6	11.3	5.5	11.5	5.8	11.4	5.5	13.6	5.4	
≤40°	11.5	5.1	9.7	5.1	9.7	5.1	8.2	5.1	8.2	5.1	9.7	5.1	9.7	5.1	11.5	5.1	
>75°	10.5	6.8	12.8	7.7	16.8	7.0	11.0	7.2	10.8	6.9	13.1	6.4	12.7	7.2	13.2	7.0	
70-75°	11.4	6.1	15.2	8.3	18.0	7.6	12.9	7.4	11.8	7.0	14.1	6.5	15.7	7.4	15.5	6.8	
65-70°	12.8	7.8	21.4	9.5	21.1	10.5	16.8	7.9	15.4	8.1	15.9	6.9	19.5	8.2	19.3	8.2	
60-65°	12.5	8.6	21.5	11.3	17.7	11.9	16.8	8.2	21.0	8.7	18.3	7.8	22.0	9.1	23.6	9.2	
55-60°	12.3	6.9	16.6	7.9	12.4	8.3	11.8	6.3	15.7	7.6	13.7	6.5	15.1	8.7	17.2	7.3	Summer
50-55°	12.0	6.7	15.6	6.9	11.8	7.2	10.4	6.0	12.9	7.2	11.6	6.1	12.3	8.6	14.1	6.9	
45-50°	11.8	6.1	13.6	6.3	11.0	6.4	9.6	5.6	11.3	6.4	11.0	5.8	11.4	7.4	13.2	6.3	
40-45°	11.6	5.6	11.6	5.6	10.4	5.8	8.8	5.4	9.7	5.8	10.4	5.4	10.5	6.3	12.3	5.6	
≤40°	11,5	5.1	9.7	5.1	9.7	5.1	8.2	5.1	8.2	5.1	9.7	5.1	9.7	5.1	11.5	5.1	

Winter: Nov, Dec, Jan, Feb in the N. hemisphere and May, Jun, Jul, Aug in the S. hemisphere.
Summer: May, Jun, Jul, Aug in the N. hemisphere and Nov, Dec, Jan, Feb in the S. hemisphere.
Equinox: Mar, Apr, Sep, Oct in both hemispheres.

REFERENCES

AGY, V. [1972] A model for the study and prediction of auroral effects on HF radar, in *"Radar propagation in the Arctic"*. Ed. J. Frihagen 32-1, AGARD Conference Proceedings 97, Technical Editing and Reproduction Ltd., London.

BARGHAUSEN, A. F., FINNEY, J. W., PROCTOR, L. L. and SCHULTZ, L. D. [1969] Predicting long-term operational parameters of high-frequency sky-wave telecommunication systems. ESSA Tech. Rep. ERL 110-ITS 78, US Government Printing Office, Washington.

BECKMANN, B. [1967] Notes on the relationship between the receiving-end field strength and the limits of the transmission frequency range MUF-LUF. *NTZ-Comm. J.*, **6** (1), 37-47.

BRADLEY, P. A. [1968] Wave polarisation and its influence on the power available from a radio signal propagated through the ionosphere — 2. *Proc. IEE*, **115** (6), 777-781.

BRADLEY, P. A. [1970] Focusing of radio waves reflected from the ionosphere at low angles of elevation. *Electronics Letters*, **6**, 457-458.

BRADLEY, P. A. and BRAMLEY, E. N. [1971] Wave polarisation and its influence on the power available from a radio signal propagated through the ionosphere — 3. *Proc. IEE*, **118** (9), 1190-1196.

BRADLEY, P. A. and DUDENEY, J. R. [1973] A simple model of the vertical distribution of electron concentration in the ionosphere. *J. Atmos. Terr. Phys.*, **35**, 2131-2146.

BRADLEY, P. A. and MURPHY, J. A. [1974] A method of prediction of median HF oblique sky-wave propagation modes and field strengths. Part. 1. Technical basis and sample results. CCIR IWP 6/1, Doc. J.

BRADLEY, P. A. and BEDFORD, C. [1976] Prediction of HF circuit availability. *Electronics Letters*, **12**, 32-33.

DAMBOLDT, T. [1976] A comparison between the Deutsche Bundespost ionospheric HF radio propagation predictions and measured field strengths, in *Radio systems and the ionosphere*. Ed. W. T. Blackband, 12-1, AGARD Conference Proceedings 173, Technical Editing and Reproduction Ltd., London.

DIEMINGER, W. and ROSE, G. [1961] Zum Feldstarkeverlauf am Rande der toten Zone (On the variation of field strength near the border of the skip zone). *NTZ*, **14**, 492-495.

DIEMINGER, W., ROSE, G. and WIDDEL, H. U. [1966] On the existence of anomalous radio wave absorption during winter in 40° northern latitude. *J. Atmos. Terr. Phys.*, **28**, 317-318.

EYFRIG, R. [1974] Comment on the ionosphere model by Bradley and Dudeney. CCIR IWP 6/1, Doc. H.

FOPPIANO, A. J. [1975] A new method for predicting the auroral absorption of HF sky waves. CCIR IWP 6/1, Docs. 3 and 10.

GEORGE, P. L. [1971] The global morphology of the quantity $\int Nv\, dh$ in the D- and E-regions of the ionosphere. *J. Atmos. Terr. Phys.*, **33**, 1893-1906.

GEORGE, P. L. and BRADLEY, P. A. [1973] Relationship between HF absorption at vertical and oblique incidence. *Proc. IEE*, **120** (11), 1355-1361.

GEORGE, P. L. and BRADLEY, P. A. [1974] A new method of predicting the ionospheric absorption of high frequency waves at oblique incidence. *Telecommunication Journal*, **41** (5), 307-312.

HAKURA, Y. [1965] Tables and maps of geomagnetic coordinates corrected by the higher order spherical harmonic terms. *Rep. Ion. and Space Res.*, Japan, **19** (2), 121-157.

HALLEY, P. [1965] Méthode de calcul des prévisions de point à point aux distances comprises entre 2500 et 10 500 km. Centre national d'études des télécommunications, Division des prévisions ionosphériques, France.

HARNISCHMACHER, E. A. [1960] A calculation method of ionospheric propagation conditions for very high and antipode distance. *Electromagnetic Wave Propagation*, Academic Press, London, 527.

HARTZ, T. R. and BRICE, N. M. [1967] The general pattern of auroral particle precipitation. *Planet. Space Sci.*, **15**, 301-329.

HAYDON, G. W., LEFTIN, M. and ROSICH, R. [1976] Predicting the performance of high frequency sky-wave telecommunication systems. (The use of the HFMUFES4 program) OT Report 76-102, US Government Printing Office, Washington.

HORTENBACH, K. J. and ROGLER, F. [1979] On the propagation of short waves over very long distances: predictions and observations. *Telecommunication Journal*, **46** (6), 320-327.

JENSEN, D. C. and CAIN, J. C. [1962] Interim geomagnetic field. *J. Geophys. Res.*, **9**, 3568-3569.

JONES, W. B., GRAHAM, R. P. and LEFTIN, M. [1969] Advances in ionospheric mapping by numerical methods. ESSA Tech. Rep. ERL 107-ITS 75, US Government Printing Office, Washington.

JONES, W. B. and OBITTS, D. L. [1970] Global representation of annual and solar cycle variation of foF2 monthly median 1954-1958. Telecomm. Res. Rep. OT/ITSRR 3, US Government Printing Office, Washington.

KANAYA, S. and WAKAI, N. [1976] Method for estimating the signal strength of ground-scatter modes at frequencies above the classical MUF for transmitter-receiver separations beyond 4000 km. CCIR IWP 6/1, Doc. 39.

KASANTSEV, A. N. [1947] The absorption of short radio waves in the ionosphere and the field strength at the place of reception. Translation (July 1958) from *Bulletin of Academy of Sciences of the USSR*. Division of Technical Sciences, **9**, 1107-1138.

KASANTSEV, A. N. [1956] Developing a method of calculating the electrical field strength of short radio waves. Trudy IRE, Transactions of the Institute of Radio Engineering and Electronics of the Academy of Sciences, USSR, **2**, 134.

KASANTSEV, A. N. [1957] Instructions for the calculation of the coefficients of ionospheric absorption and field intensity of short radio waves. Working Group of CCIR (Lepechinsky group), Geneva.

KING, J. W. and SLATER, A. J. [1973] Errors in predicted values of foF2 and hmF2 compared with the observed day-to-day variability. *Telecommunication Journal*, **40** (12), 766-770.

LAITINEN, P. O. and HAYDON, G. W. [1950] Analysis and prediction of sky-wave field intensities in the high frequency band. Technical Report 9. US Army Signal Radio Propagation Agency, Ft. Monmouth, N.J.

LEFTIN, M., OSTROW, S. M. and PRESTON, C. [1967] Numerical maps of monthly median h'F,F2 for solar-cycle minimum and maximum. Institutes for Environmental Research Tech. Mem. 69, Boulder, Colorado.

LEFTIN, M., OSTROW, S. M. and PRESTON, C. [1968] Numerical maps of foEs for solar cycle minimum and maximum. ESSA Tech. Rep. ERL 73–ITS 63, US Government Printing Office, Washington.

LITTLE, C. G. and LEINBACH, H. [1959] The riometer—a device for the continuous measurement of ionospheric absorption. *Proc. IRE*, **47** (2), 315-320.

LLOYD, J. L. [1975] Propagation loss model for modes from ionospheric irregularities. CCIR IWP 6/1, Doc. 18.

LUCAS, D. L. and HAYDON, G. W. [1966] Predicting statistical performance indexes for high frequency ionospheric telecommunications systems. ESSA Tech. Rep. IER1-ITSA1. US Government Printing Office, Washington.

MAEDA, K. [1969] Mid-latitude electron density profile as revealed by rocket experiments. *J. Geomag. Geoelect.*, **21** (2), 557-567.

MAEDA, K. [1971] Study electron density profile in the lower ionosphere. *J. Geomag. Geoelect.*, **23** (2), 133-159.

MIYA, K., KOBAYASHI, T. and WAKAI, N. [1951] Field intensity of scattered wave in radio wave propagation. *Rep. Ion. Res.*, Japan, **5** (2), 55-73.

MIYA, K. and KANAYA, S. [1955] Radio propagation prediction considering scattering wave on the earth's surface. *Rep. Ion. Res.*, Japan, **9** (1), 1-15.

MIYA, K., ISHIKAWA, M. and KANAYA, S. [1957] On the bearing of ionospheric radio waves. *Rep. Ion. Res.*, Japan, **11** (3), 130-144.

MIYA, K. and KAWAI, M. [1959] Propagation of long-distance HF signals. *Elect. and Radio Eng.*, **36**, 263-272.

MIYA, K. and SASAKI, T. [1966] Characteristics of ionospheric Es propagation and calculation of Es signal strength. *Radio Science*, **1** (1), 99-108.

MIYA, K., SCHIMIZU, K. and KOJIMA, T. [1978] Oblique-incidence sporadic-E propagation and its ionospheric attenuation. *Radio Science*, **13** (3), 559-570.

MOORAT, A. J. G. [1968] Wave polarisation and its influence on the power available from a radio signal propagated through the ionosphere — 1. *Proc. IEE*, **115** (6), 771-776.

MUGGLETON, L. M. [1975] A method of predicting foE at any time and place. *Telecommunication Journal*, **42** (7), 413-418.

NBS [1948] Ionospheric Radio Propagation. National Bureau of Standards, Circular 462, US Government Patents Office, Washington.

PIGGOTT, W. R. [1959] The calculation of the median sky-wave field strength in tropical regions. DSIR Radio Research Special Report No. 27, HMSO, London.

PIGGOTT, W. R. and RAWER, K. [1972] URSI Handbook of ionogram interpretation and reduction. Report UAG-23, World Data Center for solar-terrestrial physics, NOAA, Boulder, Colorado.

RAO, M. K. [1969] Nomographs for calculation of field strength. *J. Inst. Telecomm. Engrs.*, India, **15**, 729-740.

RAWER, K. [1952] Calculation of sky-wave field strength. *Wireless Engineer*, **29**, 287-301.

ROTTGER, J. and SCHWENTEK, H. [1974] A numerical description of the winter anomaly in ionospheric absorption for a sunspot cycle. *J. Atmos. Terr. Phys.*, **36**, 363-366.

RUSH, C. M. and GIBBS, J. [1973] Predicting the day-to-day variability of the midlatitude ionosphere for application to HF propagation predictions. AFCRL Tech. Rep. 73-0335, 2-9. Defense Documentation Center, Alexandria, Va.

RUSH, C. M., MILLER, D. and GIBBS, J. [1974] The relative daily variability of foF2 and hmF2 and their implications for HF radio propagation. *Radio Science*, **9**, 749-756.

RUSH, C. M. and ELKINS, T. J. [1975] An assessment of magnitude of the F-region absorption on HF radio waves using realistic electron density and collision frequency models. *Telecommunication Journal*, **42** (8), 476-488.

SAMUEL, J. C. and BRADLEY, P. A. [1975] A new form of representation of the diurnal and solar-cycle variations of ionospheric absorption. *J. Atmos. Terr. Phys.*, **37**, 131-141.

SCHWENTEK, H. [1966] The determination of absorption in the ionosphere by recording the field strength of a distant transmitter. *Ann. de géophys.*, **22** (2), 276-288.

SCHWENTEK, H. [1967] The trend of the amount of winter anomaly of ionospheric absorption from 1956 till 1966. *J. Atmos. Terr. Phys.*, **29**, 1169-1173.

SCHWENTEK, H. [1968] Zum Auftreten der Winteranomalie der ionosphärischen Absorption von Kurzwellen. *NTZ*, **21**, 32-39.

SCHWENTEK, H. [1971] Regular and irregular behaviour of the winter anomaly in ionospheric absorption. *J. Atmos. Terr. Phys.*, **33**, 1647-1650.

SINNO, K., KAN, M. and HIRUKAWA, Y. [1976] On the reflection and transmission losses for ionospheric radio wave propagation via sporadic E. *J. Radio Res. Labs.*, Japan, **23** (110), 65-84.

STEWART, F. G. and LEFTIN, M. [1972] Relationship between Ottawa 10.7 cm solar radio noise flux and Zurich sunspot number. *Telecommunication Journal*, **39** (3), 159-169.

TIFFON, J. [1974] La prévision de la médiane mensuelle foE et la limite supérieure des fréquences réfléchies par la couche E normale, entre deux points au sol. Rapport Technique EST/DPI/887, Centre national d'études des télécommunications, Issy-les-Moulineaux.

TITHERIDGE, J. E. [1958] Variations in the direction of arrival of high frequency radio waves. *J. Atmos. Terr. Phys.*, **13**, 17-25.

TURUNEN, T. [1975] Measuring the echo amplitudes of sporadic E layer in swept frequency ionospheric sounding. *Geophysica*, **13** (2), 167-173.

WAKAI, N. [1961] Non-deviative absorption at night. *J. Radio Res. Labs.*, Japan, **8** (37), 213-218.

WAKAI, N. [1971] Study on the night-time E region and its effects on the radio wave propagation. *J. Radio Res. Labs.*, Japan, **18** (98), 245-348.

WAKAI, N. [1975] Nomogram for easy readout of the night-time absorption. CCIR IWP 6/1, Doc. 12.

WAKAI, N., OUCHI, C. and NEMOTO, C. [1970] Winter anomaly of ionospheric absorption as observed in Loran-A signals. *J. Radio Res. Labs.*, Japan, **17** (91), 185-198.

WAKAI, N., OSE, M. and TANOHATA, K. [1971] Solar control of HF radio wave absorption in the night-time. *J. Radio Res. Labs.*, Japan, **18** (95), 1-17.

WAKAI, N., OUCHI, C. and NEMOTO, C. [1974] Spatial extent of the winter anomaly in absorption, in *Methods of measurements and results of lower ionosphere structure.* Ed. K. Rawer, 307-311. Akademie-Verlag, Berlin.

WHEELER, J. L. [1966] Transmission loss for ionospheric propagation above the standard MUF. *Radio Science*, **1** (11), 1303-1308.

ZACHARISEN, D. H. and CROW, E. L. [1970] Fitting distributions of telecommunication variables with chi-square distributions. *Radio Science*, **5** (11), 1307-1315.

ZACHARISEN, D. H. and JONES, W. B. [1970] World maps of atmospheric noise in universal time by numerical mapping. OT/ITS Res. Rep. 2, US Government Printing Office, Washington.

CCIR Document

[1970-74]: 6/65 (Japan).

BIBLIOGRAPHY

TURUNEN, T. [1974] Gain sensitive parameters. URSI Ionospheric Network Advisory Group Bulletin, **17**, 4 and 18, 12-16.

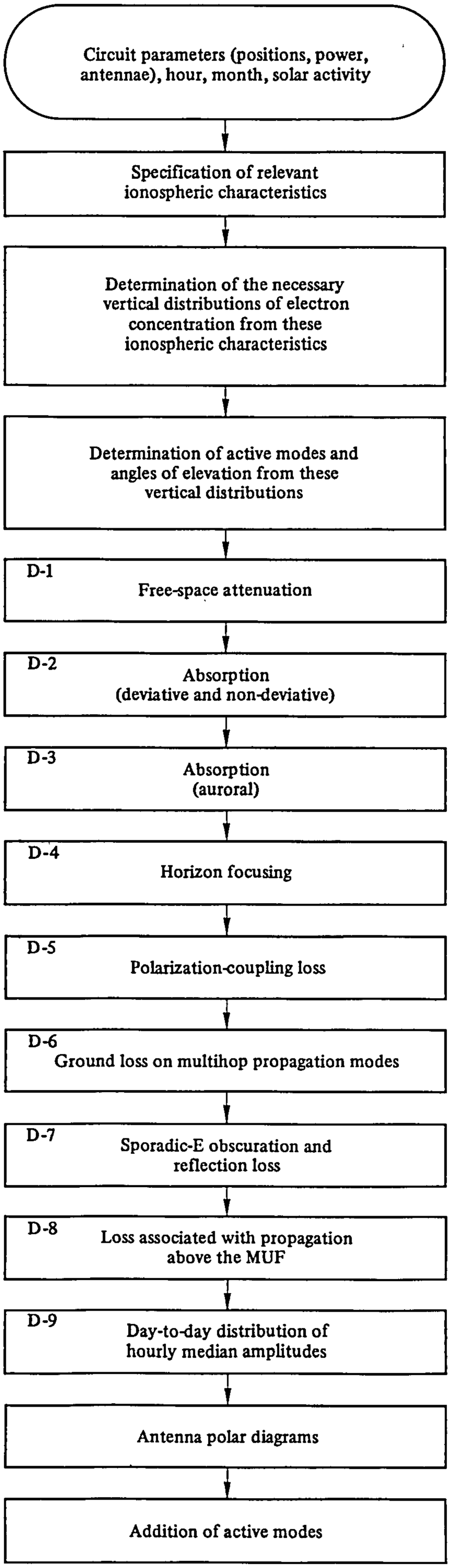

FIGURE 1 – *Summary of proposed procedures for field-strength and transmission-loss determination given in Report 572 (Geneva, 1974)*

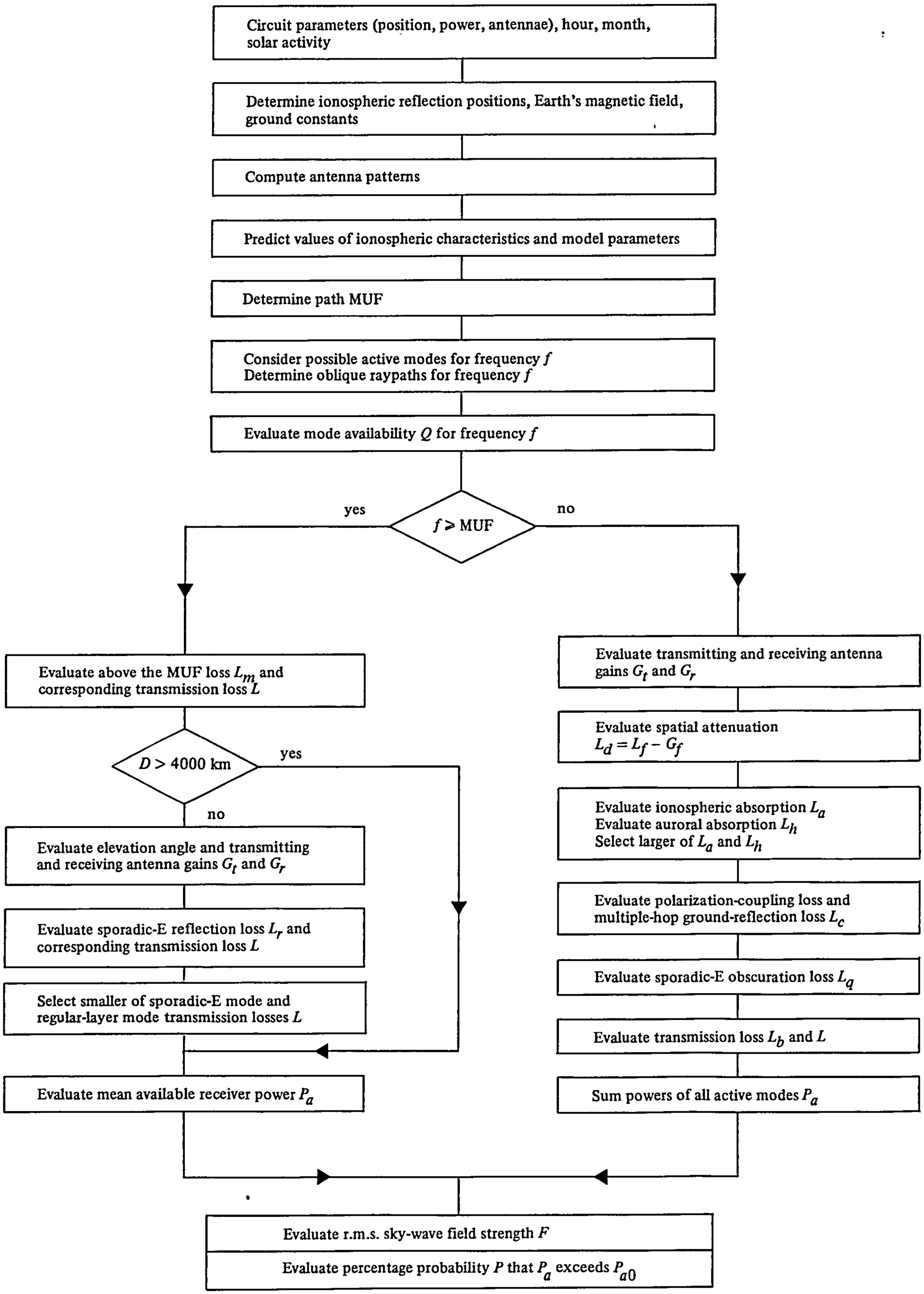

FIGURE 2 — *Simplified schematic representation of the stages of computation of the overall transmission loss, r.m.s. sky-wave field strength and mean available receiver power*

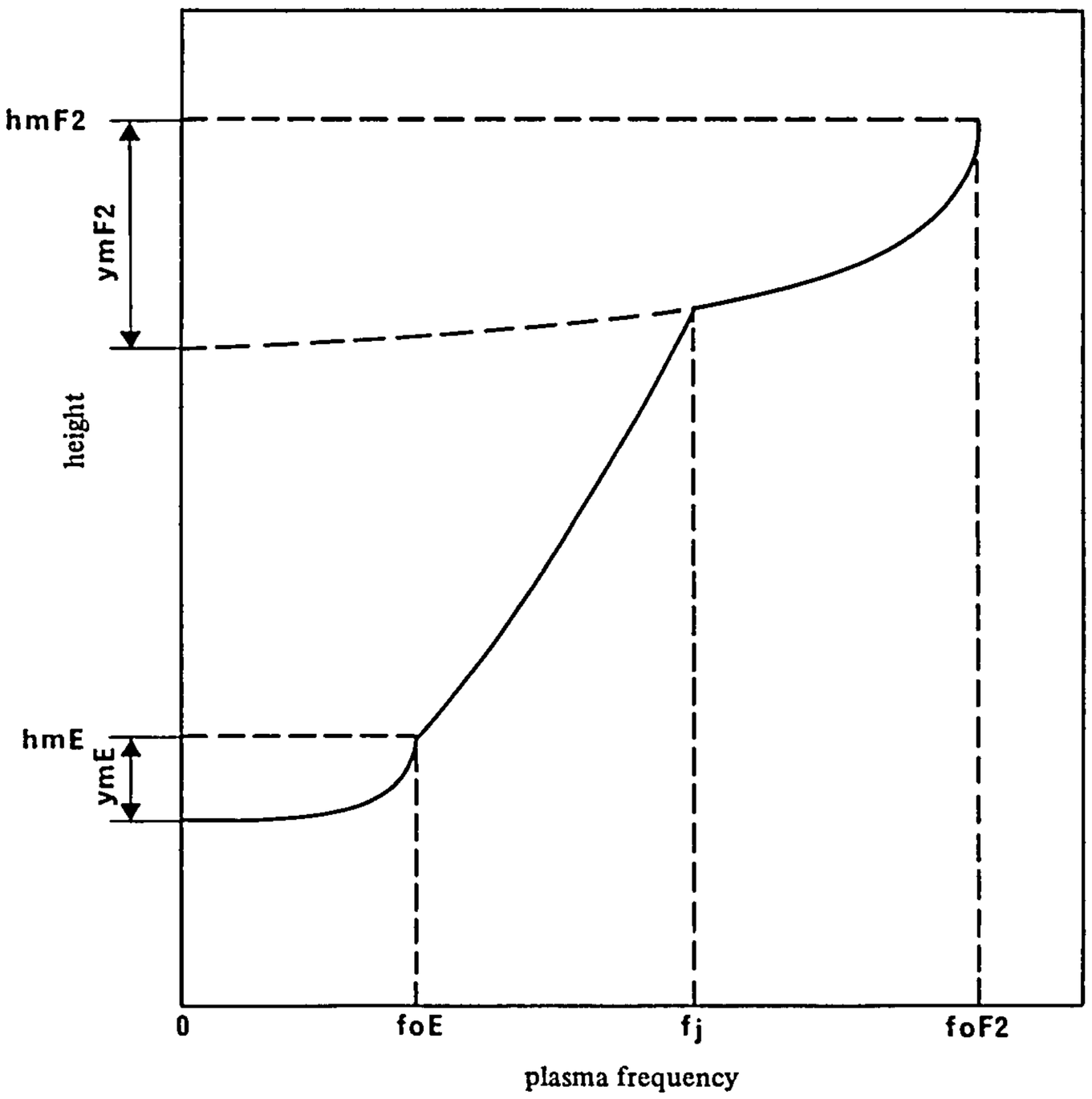

FIGURE 3 — *Idealized model of vertical distribution of electron concentration*

This consists of:

— a parabolic E-layer

— a linear increase of electron concentration with height in the Fl-region, and

— a parabolic F2-layer

The ordinate scale is taken as being linear in height and the abscissa as linear in frequency.

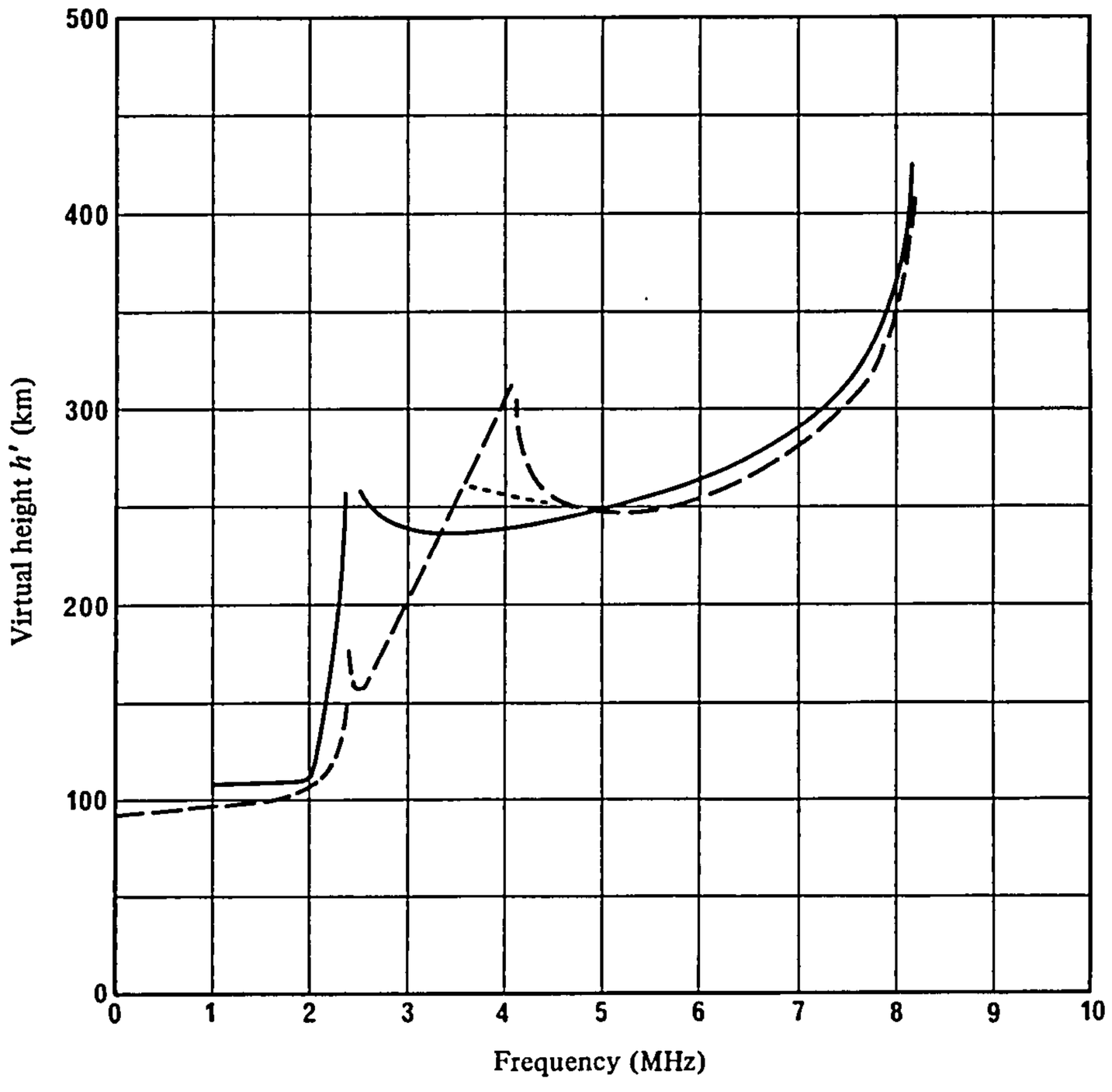

a)

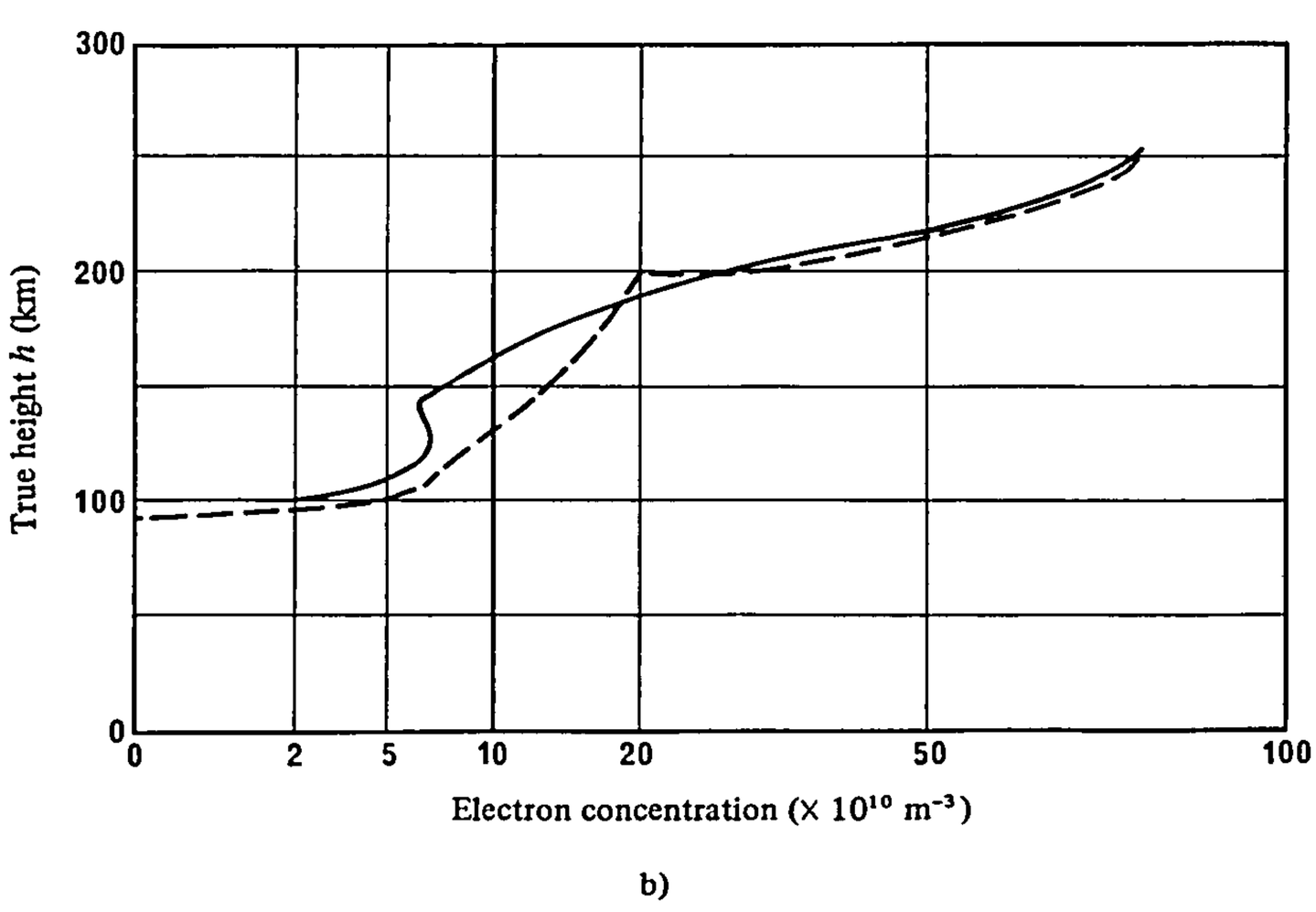

b)

FIGURE 4 — *Example showing (a) ionogram recorded at Argentine Islands at 16.45 LT on 29 September, 1958, and (b) associated electron-concentration height distribution derived by true-height analysis*

These are compared with the corresponding height distributions for the model and with its associated synthesized ionogram produced using the equations indicated.

(*a*) ———— measured ionogram

— — — — ionogram synthesised using equations (14), (16) and (18)

. . . . . portion of ionogram synthesized using equation (20)

(*b*) ———— from true-height analysis

— — — — from model

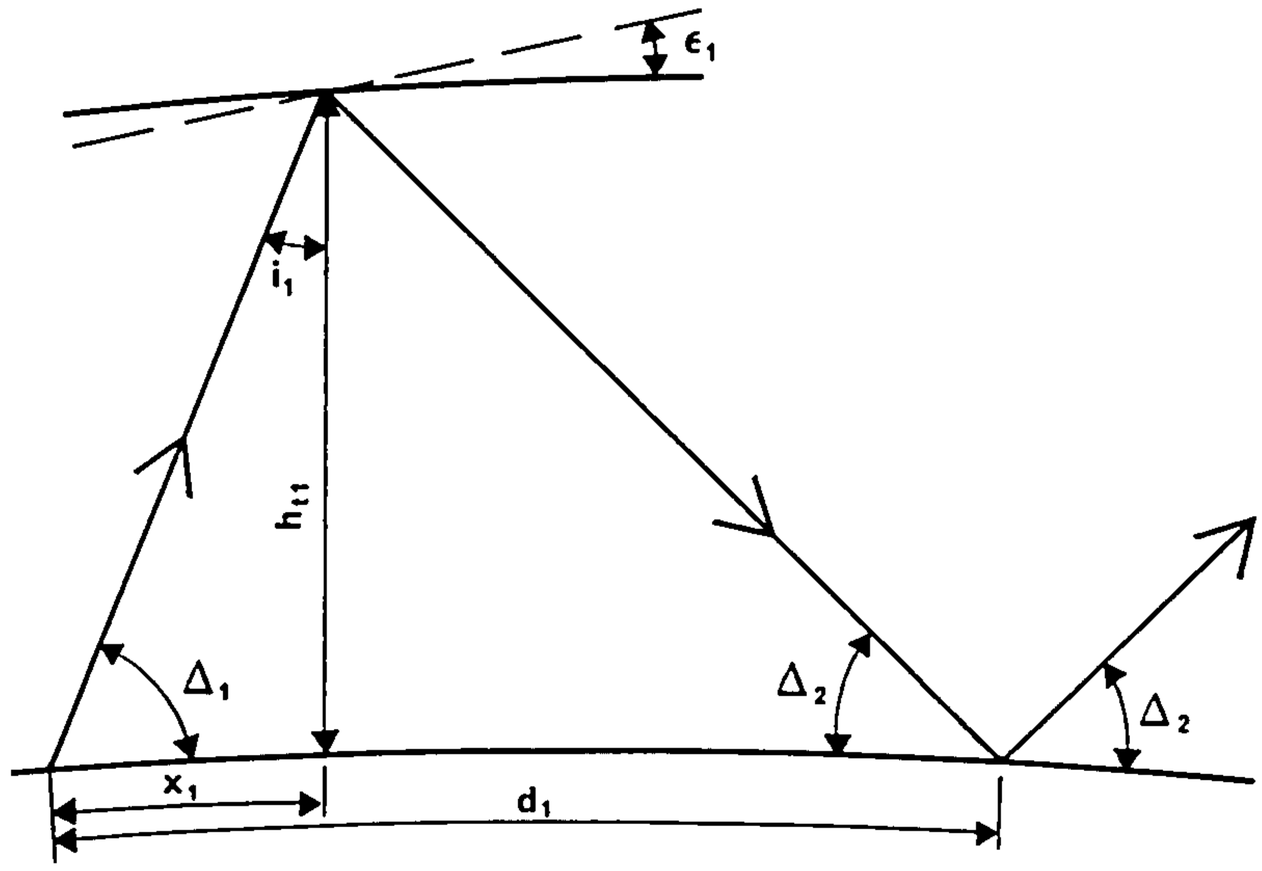

FIGURE 5 — *Ray-hop geometry*

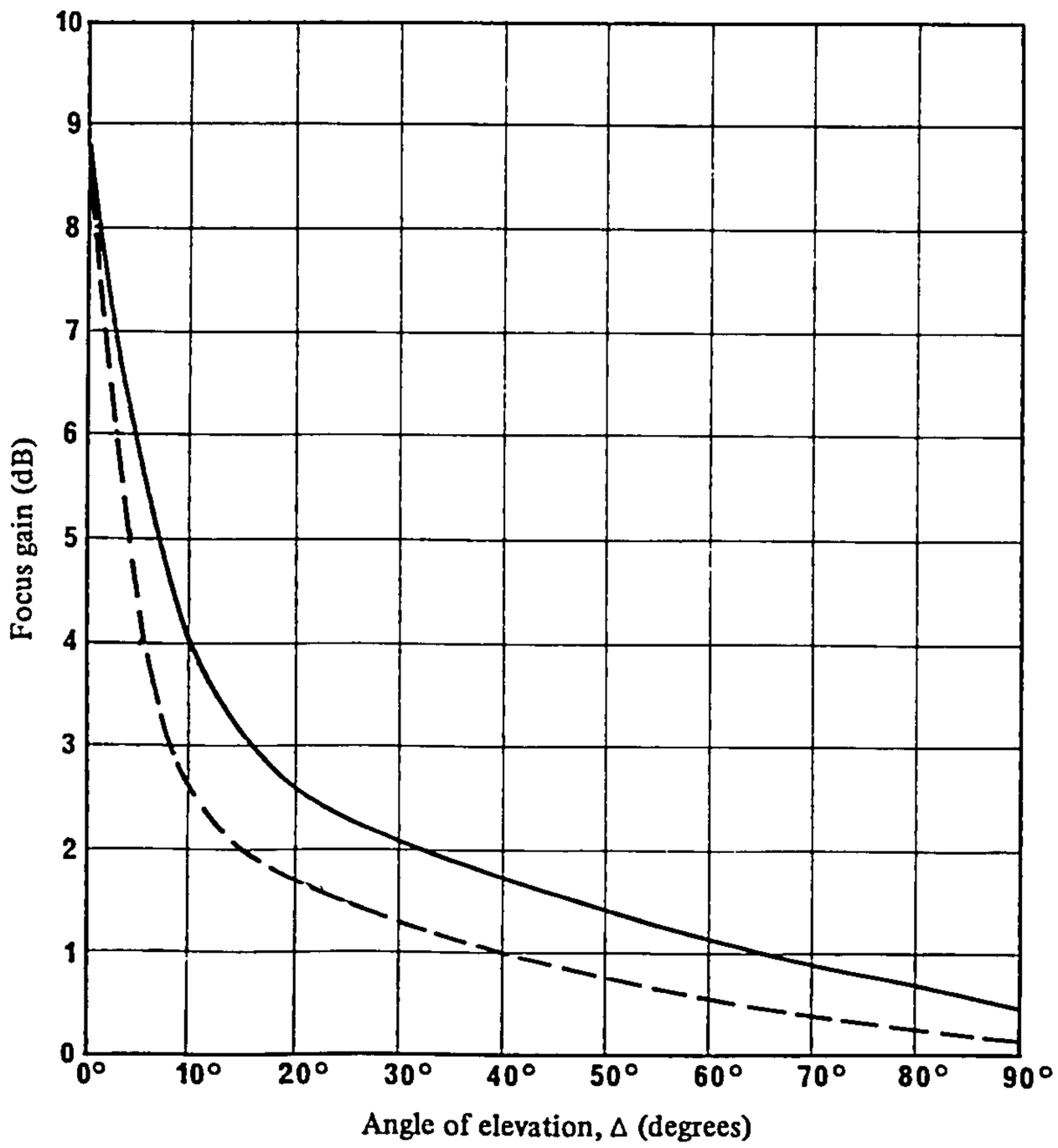

FIGURE 6 — *Horizon-focus gain, G_f*

——————— F modes

— — — — — E modes

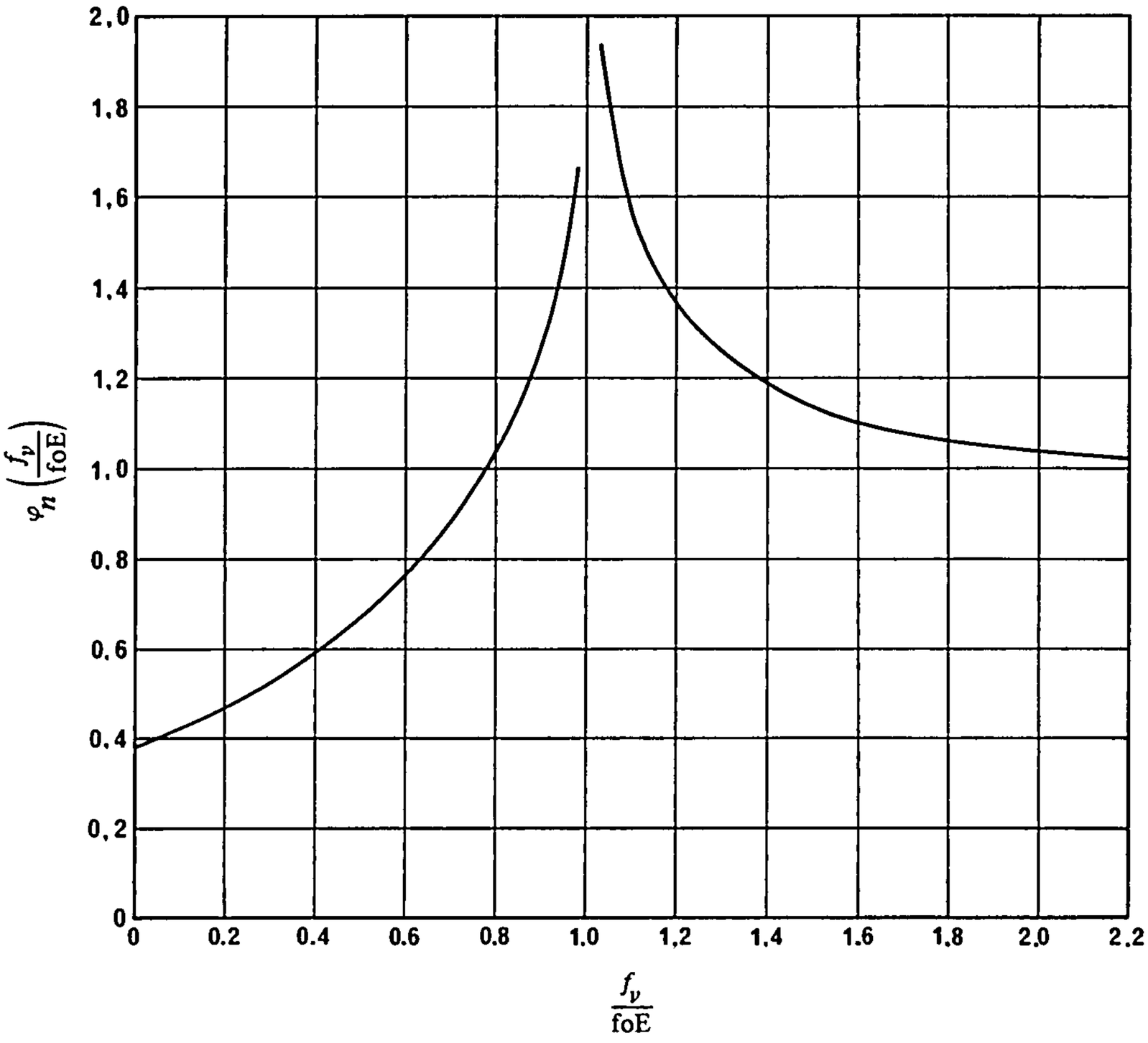

FIGURE 7 — *The absorption factor* $\varphi_n\left(\frac{f_\nu}{\text{foE}}\right)$

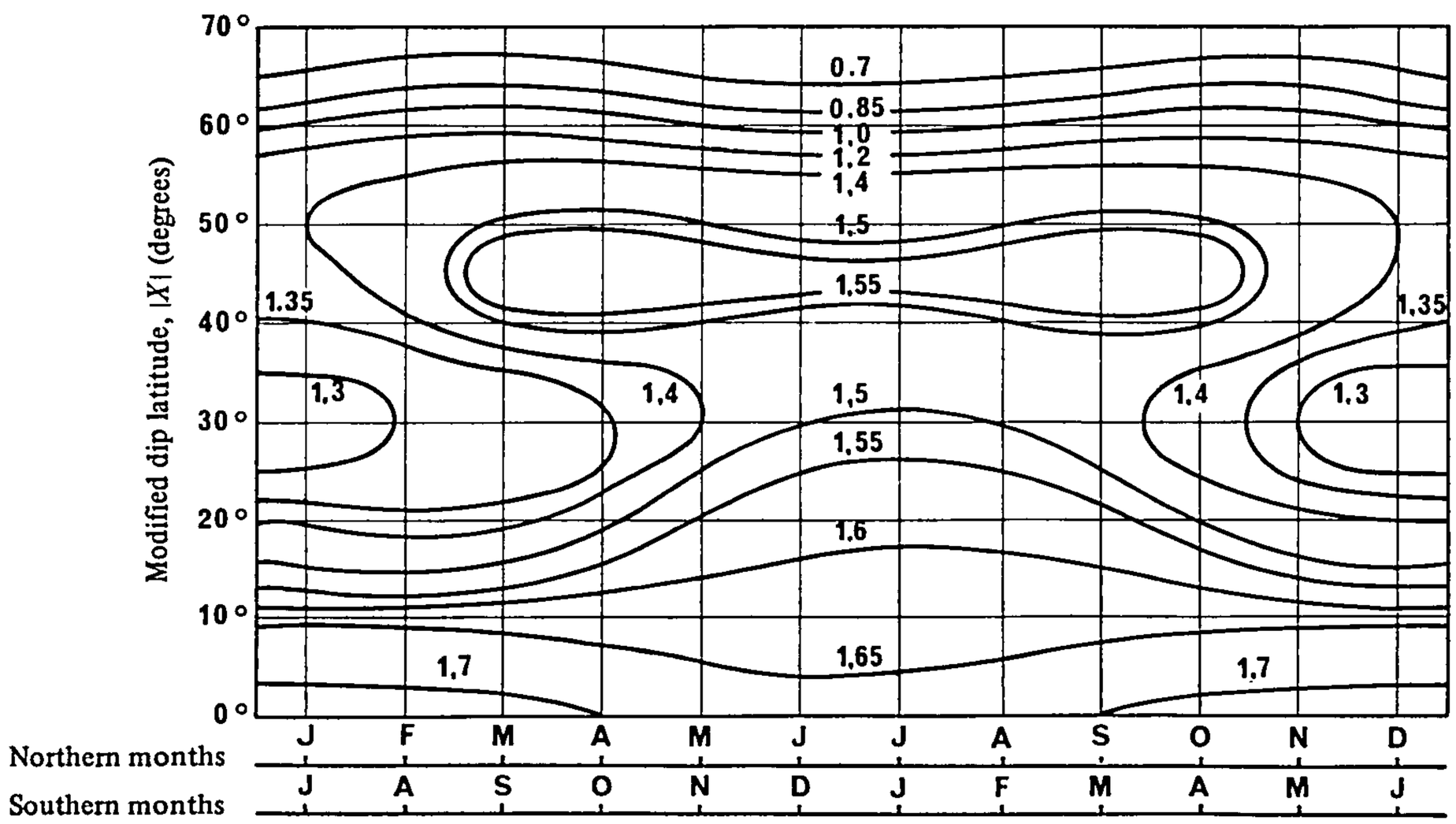

FIGURE 8 — *The diurnal absorption exponent p*

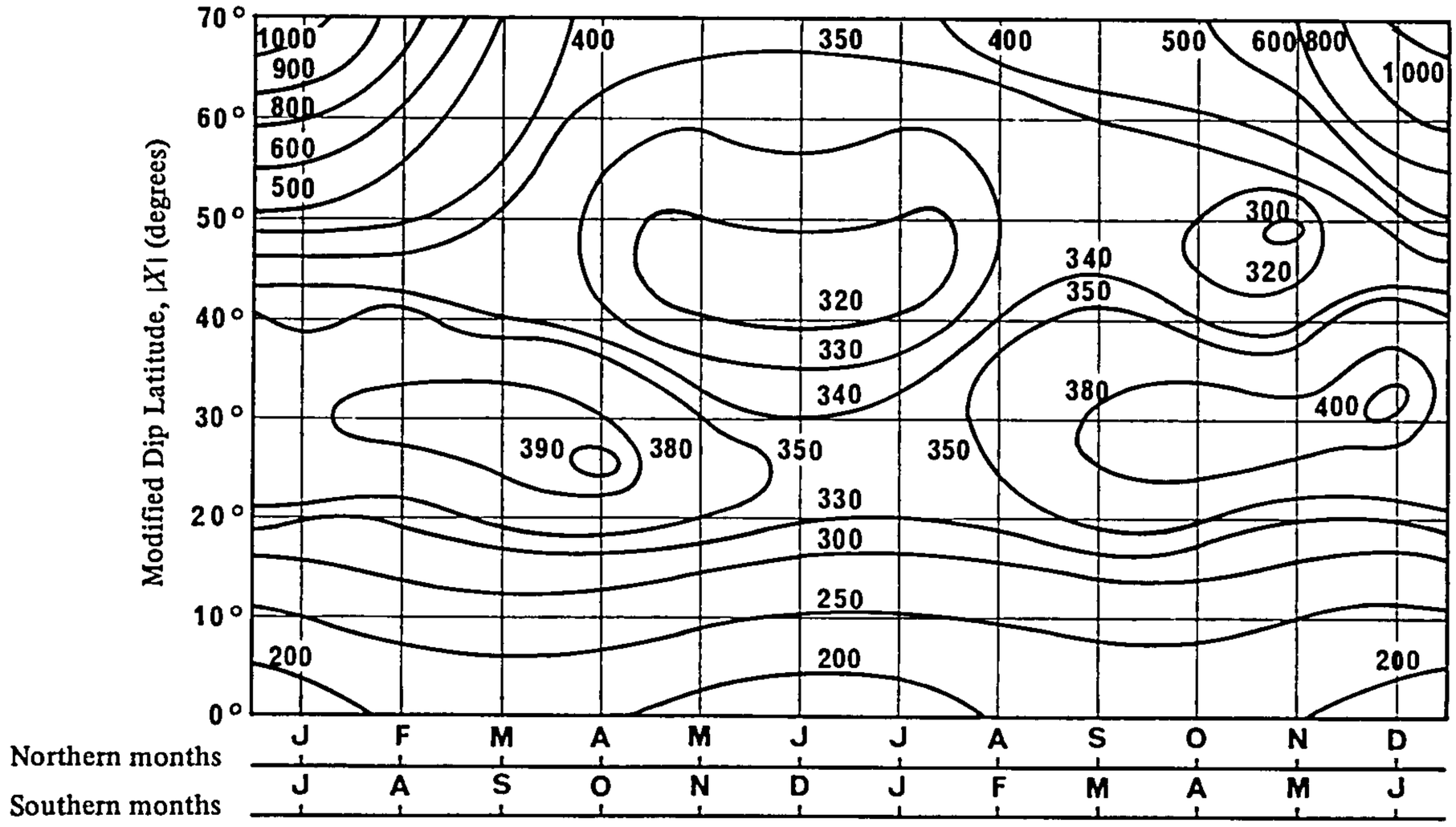

FIGURE 9 — *The absorption factor, A_T(0,0)*

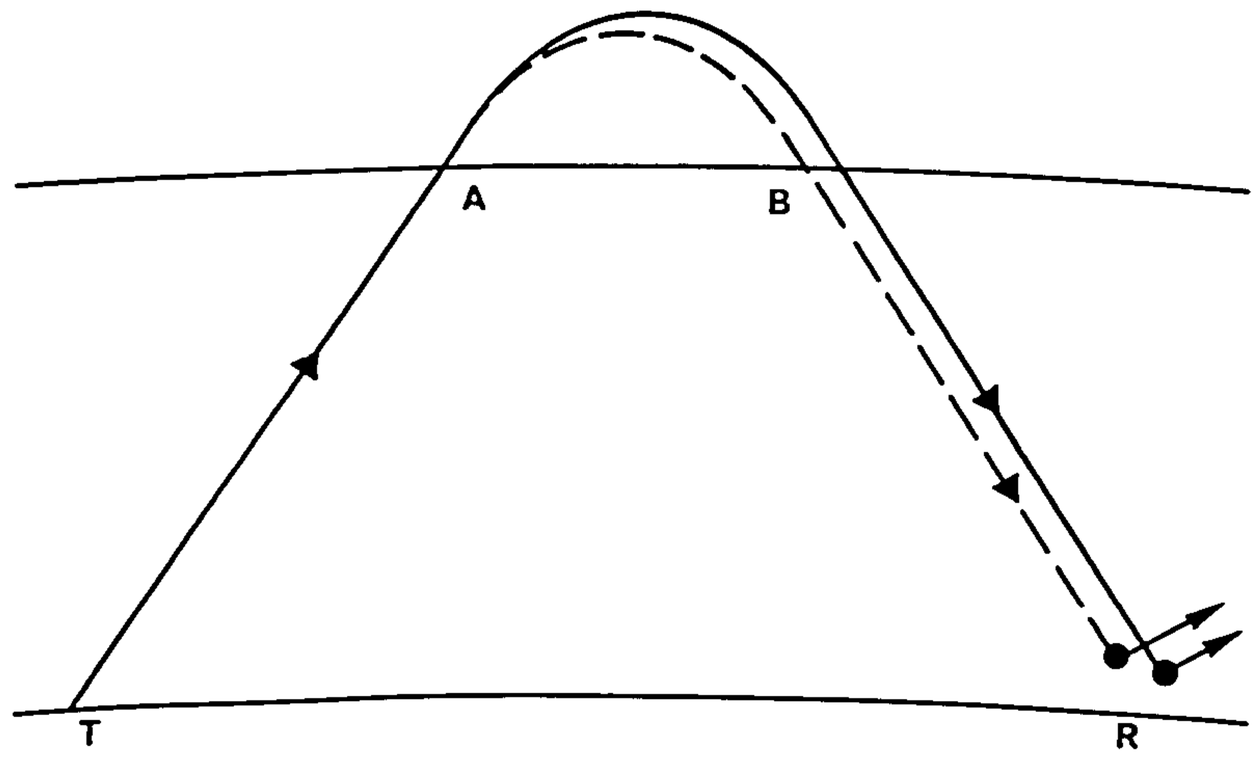

FIGURE 10 — *Single-hop ray path geometry for polarization-coupling loss determination*

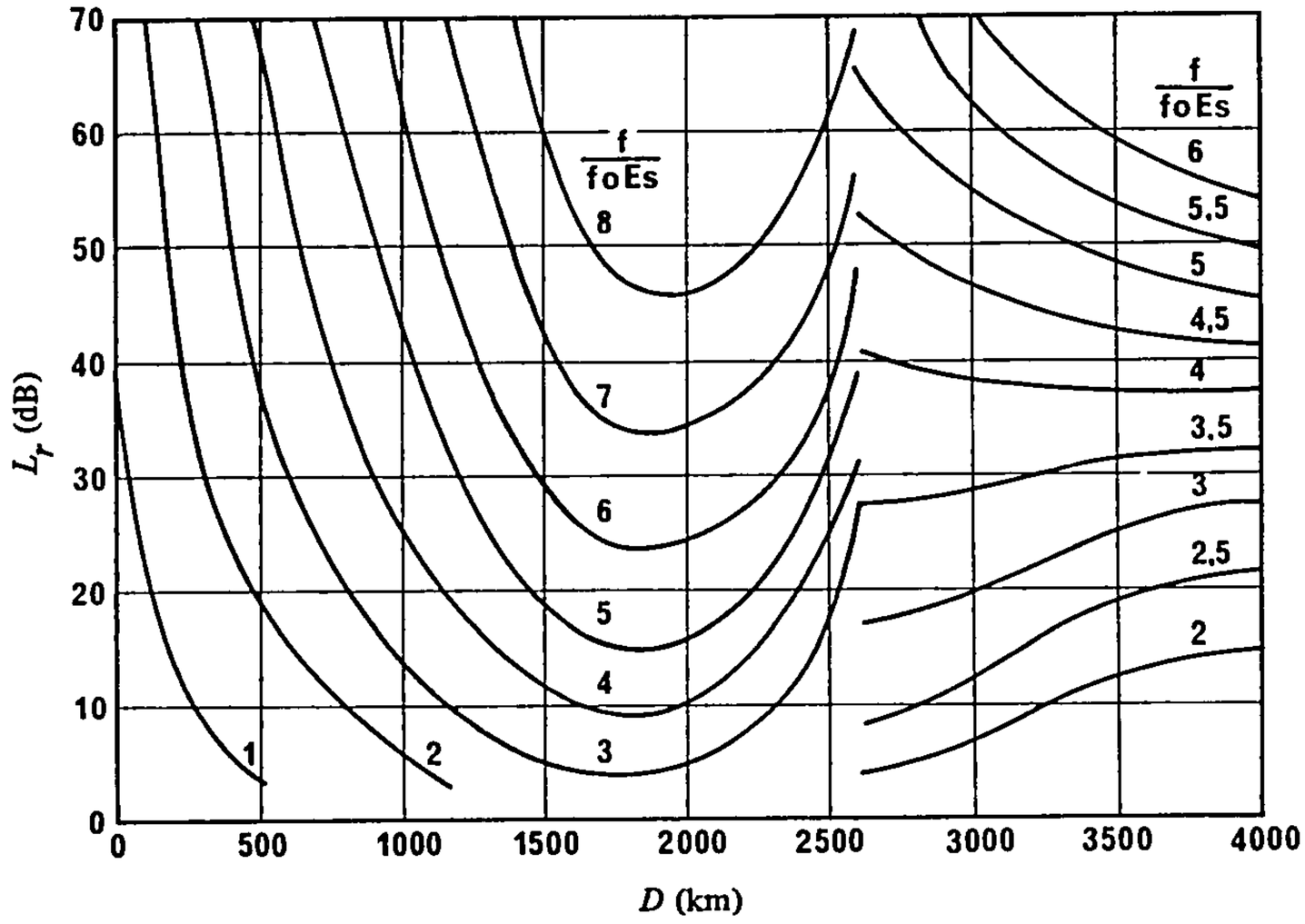

FIGURE 11 — *Sporadic-E reflection loss, L_r*